STATE RESEARCH CENTER OF RUSSIA

INSTITUTE FOR HIGH ENERGY PHYSICS

IHEP 96-98

Proposal

AN EXPERIMENT FOR STUDYING MECHANISMS OF CHARMED PARTICLE PRODUCTION AND DECAYS IN pA-INTERACTIONS AT 70 GEV/C

E.Ardashev, M.Bogolyubsky, N.Bulgakov, V.Burtovoy, S.Chekulaev, V.Chmill, A.Chuntonov, Yu.Tsyupa, E.Eremchenko, A.Gavlitsky, N.Galyaev, V.Golovkin, N.Ivanova, V.Khmelnikov, A.Kholodenko, A.Kiryunin, V.Klyukhin, V.Konstantinov, V.Komarov, L.Kurchaninov, M.Levitsky, A.Mayorov, V.Maximov, A.Minaenko, A.Moiseev, A.Pleskach, A.Popov, Yu.Rodnov, V.Ryadovikov, S.Sidorov, A.Smoll, V.Solomko, A.Vorobiev, O.Zaitseva, V.Zapolsky, V.Zmushko, I.Zubkov
Institute for High Energy Physics, Protvino, Russia

N.Amaglobeli, B.Chiladze, L.Demetrashvili, I.Trekov
High Energy Physics Institute, Tbilisy State University, Tbilisy, Georgia

S.Basiladze, G.Bogdanova, O.Deryugin, P.Ermolov[1], Ya.Grishkevich, A.Kalagov, B.Kozlov, V.Kramarenko, A.Kubarovsky, A.Larichev, A.Leflat, S.Orfanitsky, V.Rybnikov, A.Selikov, L.Tikhonova, A.Vischnevskaya, V.Volkov, S.Zotkin
Nuclear Physics Institute, Moscow State University, Moscow, Russia

I.Boguslavsky, V.Bychkov, N.Dikusar, P.Eremeev, O.Gavrizchyuk, I.Gramenitsky, A.Ivanov, Yu.Ivan'shin, A.Yukaev, E.Kazarenko, G.Kekelidze, V.Kireev, A.Kolomyichenko, I.Kosarev, A.Kutov, S.Lobastov, V.Lysan, K.Medved, S.Misyutin, V.Novikov, A.Oleynik, V.Peshekhonov, Yu.Petukhov, V.Samsonov, M.Shafranov, A.Shalygin, S.Suchkov, V.Tolmachev, T.Topuria
Joint Institute for Nuclear Research, 141980 Dubna, Russia

[1]Spokesman

Protvino 1996

UDK 539.1.07 M–24

Abstract

Ardashev E., Bogolyubsky M., Bulgakov N. et al. PROPOSAL. An Experiment For Studying Mechanisms of Charmed Particle Production and Decays in pA-Interactions at 70 GeV/c: IHEP Preprint 96–98. – Protvino, 1996. – p. 47, figs. 24, tables 7, refs.: 52.

In the proposal of an experiment the aimes of a continuation of charm particle production studies started in the framework of experiment E–161 with the SVD set-up are formulated. From an analysis of the existing data on charm hadroproduction obtained in fixed target experiments and of modern theoretical ideas on mechanisms of heavy quark production in hadronic collisions it is shown that conducting an experiment at the energy near the threshold of charm production offers an unique opportunity to verify the intrinsic charm hypothesis and to estimate a possible contribution of such a mechanism to the charm particle yield. A capability of an experiment in this energy range for a study of exclusive nonleptonic decays of Λ_c^+-baryons is also envisaged. The upgrade for the SVD set-up needed to realize the proposed program of physical investigations, including problems of fabrication of the new precision vertex detector, of the trigger system electronics and of development of the data acquisition system is considered. The results of the detailed Monte Carlo simulation of the charmed events triggering efficiency and of the probability to detect charmed hadron decays with the upgraded SVD set-up are presented. Finally the organization of the data handling system using the interactive program of the graphical analysis of events is discussed and the rate of statistics accumulation is estimated.

Аннотация

Ардашев Е.Н., Боголюбский М.Ю., Булгаков Н.К. и др. Предложение эксперимента по изучению механизмов образования очарованных частиц в pA-взаимодействиях при 70 ГэВ/с и их распадов: Препринт ИФВЭ 96–98. – Протвино, 1996. – 47 с., 24 рис., 7 табл., библиогр.: 52.

Сформулировано предложение по развитию исследований образования очарованных частиц в pA4-взаимодействиях при 70 ГэВ/с на установке СВД, начатых в рамках эксперимента Е-161. На основании анализа данных по образованию очарованных частиц, полученных в экспериментах на выведенных адронных пучках, и современных теоретических представлений о механизмах рождения тяжелых кварков в адронных столкновениях показано, что проведение исследований в околопороговой области энергий предоставляет уникальную возможность для проверки гипотезы "внутреннего" очарования и оценки предполагаемого вклада этого механизма. Получены также возможности эксперимента в этой области энергии по изучению малочастичных нелептонных распадов Λ_c^+-барионов. Рассмотрены вопросы модернизации установки СВД, необходимой для реализации предложенной программы физических исследований, которая, в первую очередь, включает создание нового прецизионного вершинного детектора, электроники триггерной системы и новой системы сбора информации. Приведены результаты детального моделирования методом Монте-Карло эффективности отбора событий с образованием $\bar{c}c$-пар с помощью предложенной триггерной системы и вероятностей регистрации в модернизированной установке продуктов распада очарованных мезонов и барионов. В заключение рассмотрена организация системы обработки экспериментальной информации с использованием интерактивных программ графического анализа событий и оценены темпы набора статистики.

Contents

1. INTRODUCTION

To carry out the experiment E–161 [1], approved by the XX session on SCC at IHEP, a new experimental hybrid type apparatus – Spectrometer with Vertex Detector (SVD) has to be constructed. It has been decided, that a creation of this apparatus would be accomplished in two steps, corresponding to the two stages of E–161. At the first stage of this experiment a rapid cycling liquid hydrogen bubble chamber should be used as a precision vertex detector, while of the spectrometric part of the set-up only a wide aperture magnetic spectrometer with multiwire proportional chambers and hodoscopic detector of $\gamma-$quanta should be manufactured. At the second stage of the experiment it was planned to make a fast and precision vertex detector, based on the electronic technique, and to develop the spectrometer part of the set-up, in order to increase significantly (by about 100 times) the rate of data accumulation.

By this time the rapid cycling chamber, trigger system and magnetic spectrometer have been completely assembled and tested, and a few data collection runs were carried out, using the set-up in such a configuration. The commissioning of the γ-detector, consisting of Čerenkov full absorption counters, has been also finished, and so for the present the first stage of the experiment E–161 is close to completion, though because of the changed external conditions, with lower statistics, than it has been supposed.

The preliminary results, obtained at the first stage of the experiment, have been reported at the XXVII International Conference on High Energy Physics [2].

During this time both the design and electronics of the precision vertex detector with microstrip silicon detectors have been worked out, as well as the design of the elements of the second stage of the spectrometer part has been completed. Moreover, since the original proposal of E–161 had been prepared on the basis of almost 10 year old data on the charm hadroproduction, the physical tasks of the second stage of the experiment were reformulated, taking into account modern theoretical ideas on charm hadroproduction mechanisms in the near threshold region. All this made the submitting of an additional proposal for the second stage of E–161 relevant.

2. PHYSICAL GROUNDS

2.1. Study of charm hadroproduction mechanisms

2.1.1. Up-to-date state of the problem

According to modern theoretical ideas, the main mechanism of charmed quark production is hard scattering of two partons, which belong to colliding hadrons.

The cross section of such a hard subprocess in quantum chromodynamics (QCD) is described by the factorization equation:

$$\sigma = \sum_{ij} dx_1 dx_2 f_i(x_1, \mu) f_j(x_2, \mu) \hat{\sigma}(x_1 x_2 s, \mu^2), \tag{1}$$

where f_i, f_j are structure functions of the colliding partons i and j, estimated with a scale parameter μ. The cross section of the parton interactions at the energy in their center of mass system $\hat{s} = x_1 \cdot x_2 \cdot s$ can be calculated in the perturbation theory of QCD (PT QCD), using the expansion in powers of the strong coupling constant $\alpha_s(\mu)$ (though the c-quark is not sufficiently heavy for a rigorous proof of PT QCD formalism applicability). The $\bar{c}c$-pair production diagrams, conforming the leading term in the constant $\alpha_s(\mu)$, are given in Fig.1. At present the cross section of the inclusive production of $\bar{c}c$-pairs has been calculated, taking into account the next–to–leading term, which contribution is by a factor of three larger than that of the leading term. As follows from Fig.2, the energy dependence of the cross section of charm production in pN-interactions, as measured in the fixed target experiments carried out in CERN and FNAL [3], generally does contradict the QCD predictions (though, the data, obtained in pp-interactions at $\sqrt{s} = 62$ GeV at the storage rings of CERN, which are not shown in Fig.2, do not fit this picture [4]). The latest $\sigma_t(\bar{c}c)$ measurements at $\sqrt{s} < 12$ GeV at IHEP proton synchrotron conform well to the QCD prediction on a fast fall of charm hadroproduction cross section with energy. Results of $\sigma_t(\bar{c}c)$ measurements in hadron – nuclear interactions at the near - threshold energies, obtained in previous experiments, are analyzed in Ref. [5].

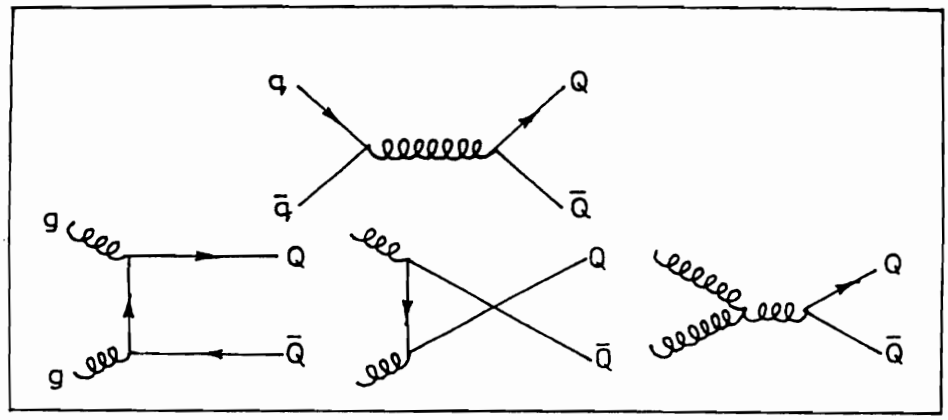

Fig. 1. $\bar{c}c$-pair production diagram, conforming to the leading term of the perturbative QCD.

However, the accuracy of a theoretical prediction of $\sigma(\bar{c}c)$ is still rather limited because of large radiation corrections, the lack of knowledge of structure functions, an uncertainty of $\bar{c}$-quark mass value, etc.

Therefore, the data on the charm production cross section in nucleon–nucleon collisions so far can not serve as a reliable proof of the predictions, made within the context of the perturbative QCD. A study of a cross section dependence on the atomic number of the nucleus appears to give better possibilities for verifying whether all the charm hadroproduction mechanisms are limited by the subprocesses, predicted by QCD. Actually, if in hA-interactions charm quarks are produced only in hard collisions of partons, then their total cross section $\sigma_t(\bar{c}c)$ must be proportional to the number of these partons. Therefore, when using the ordinary parametrization:

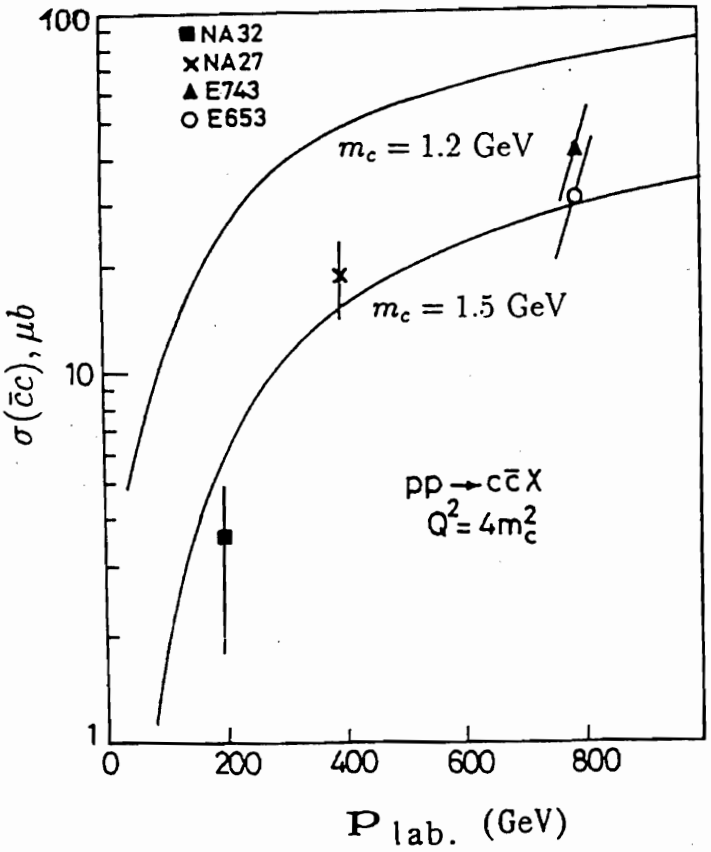

Fig. 2. Results of the calculations of $\sigma_{tot}(\bar{c}c)$, made using the perturbative QCD with the next – to – leading term.

$$\sigma = \sigma_0 \cdot A^{\alpha},$$

the parameter α for the processes, described by PT QCD, must be equal to unity.

The latest results of the α measurements in processes of "open" charm production, obtained in CERN and FNAL experiments, within the large error bars agree with this statement. For example, the experiment WA 82 [6] have shown, that the parameter α, determined for the D-meson production in $\pi^- A$-interactions at 340 GeV/c, is 0.92 ± 0.06. In $\pi^{\pm} A$-interactions at 250 GeV/c this parameter is found to be $\alpha = 1.00 \pm 0.05 \pm 0.02$ for the cross sections of D^0, $D^{\pm}$-meson production [7], and $\alpha = 1.00 \pm 0.07 \pm 0.02$ for the cross section of $D^{*\pm}$-meson production [8]. Within the limits of even larger experimental error bar no dependence of the parameter α on x_F of charms was found in these experiments.

However, in more precise experiments on hadroproduction of J/Ψ-particles, i.e. "closed" charm, where the statistics by a factor of 100 and more exceeded the one in the open charm experiments, important rules of the A-dependence of the parameter α were ascertained. Thus, the experiment NA3 [9] on the J/Ψ-particle production in

$h^{\pm} A$-interactions at 150, 200 and 280 GeV/c (where $A \equiv H_2, Pt$) showed, that the ratio $\frac{d\sigma_{H_2}}{dx_F} / \frac{d\sigma_{Pt}}{dx_F}$ increases 2-fold with the x_F growth from 0.3 to 0.9. It was also demonstrated,

that the ratio $\frac{d\sigma_{H_2}}{dp_t}/\frac{d\sigma_{Pt}}{dp_t}$ diminished $2.5 \div 3$–fold with the increase of p_t to 4 GeV/c. The authors of Ref.[9] were the first, who proposed for an explanation of these effects to introduce an additional diffraction mechanism of the $\bar{c}c$-pair production, which can not be described in the frame of the perturbative QCD, and according to their estimations is responsible for about 18% of $\sigma_t(J/\Psi)$. At present the suppressionof J/Ψ-particles yield at a large x_F has been confirmed by rich statistics in pA-interactions at 800 GeV/c (the experiment E772) [10]. This experiment has shown that in agreement with pA-data at 200 GeV/c [9], the parameter α changes from 0.95 to 0.80, as x_F of a J/Ψ-particle increases from 0 to 0.6. A value of this parameter for the total cross section of the J/Ψ-particle production, determined by using the data, obtained with four different nuclear targets, also turned out to be significantly different from unit, $\alpha = 0.92 \pm 0.01$.

A theoretical analysis shows, that the experimentally ascertained dependences of the parameter α on x_F and p_t cannot be caused by shadowing effect [11] or by a nuclear absorption [12], so at present they are considered to be a direct indication of existing of a charm quark production mechanism, different from the ones, predicted by PT QCD. Moreover, as it was shown in Ref.[13], the J/Ψ-particles, produced in $\pi^- N$-interactions, at large x_F turn out to be longitudinally polarized, which also assumes the change of their production mechanism with x_F increase.

An additional evidence on the existence of such a mechanism was obtained in investigations of the differential cross sections of particles with "open" charm. These cross sections, though so far measured with a smaller statistical accuracy, than the differential cross sections of J/Ψ-particles, unlike the last ones allow to verify the presence of correlations between a shape of spectra of charm particles with the certain quark content and the quantum numbers of the incident nucleons.

As is known from the QCD factorization theorem [14], in the leading–twist approximation the fragmentation function of a charm (as well as any other) quark, $D_{h/c}(z, Q)$, must not depend on the quantum numbers of the colliding nucleons. However, just the first accurate measurements of spectra of charmed $D-$mesons, produced in $\pi^- p$-interactions at 360 GeV/c, which were carried out in the experiment NA27, showed that $D^-(\bar{c}d)$ and $D^0(c\bar{u})$-mesons had essentially smaller values, than those of $D^+(c\bar{d})$ and $\bar{D}^0(\bar{c}u)$-mesons, of the slope parameter n of the $d\sigma/dx_F$-distributions, obtained by the approximation of them by the expression $(1 - x_F)^n$, ((1.8 ± 0.6) and (7.9 ± 1.5) respectively) [15]. This leading effect of the charm meson, containing projectile valence quark, (in the case above: a quark of $\pi^-(\bar{u}d)$-meson), recently was confirmed in a number of experiments on the charm D-meson production in $\pi^{\pm} A$-interactions.

In order to estimate a size of the leading effect in these experiments the asymmetry parameter was introduced:

$$A(x_F) = \frac{\frac{d\sigma_{lead}}{dx_F} - \frac{d\sigma_{non-lead}}{dx_F}}{\frac{d\sigma_{lead}}{dx_F} + \frac{d\sigma_{non-lead}}{dx_F}}.$$

Recent results, obtained in the experiments WA82 [16] and E769 [17], have shown, that in $\pi^- A$-interactions, the asymmetry parameter $A(x_F)$ increases from 0 to ~ 0.5, as x_F rises from 0 to 0.65.

On the qualitative level the leading effect can be explained, assuming a possibility of c-quark recombination with the primary π^--meson valence quark (anti-quark) at the stage of c-quark hadronization. Such a possibility is included, for example, in the Lund string fragmentation model. However, a comparison of the results of calculations with PYTHIA program, using the Lund model to describe a quark fragmentation, with the latest experimental data demonstrates that PYTHIA significantly overestimates a difference in the spectra of the leading and non-leading charms in the region of small and mean x_F [18].

In Refs.[18,19] it has been shown, that all of the mentioned above effects, which are beyond the perturbative QCD, can be explained by using a hypothesis of intrinsic charm. IT predicts a non zero probability of the presence in the hadron wave function of the Fock state containing a virtual $\bar{c}c$-pair, for example, for π-meson of the state $|\bar{u}d\bar{c}c>$. The life time of such $\bar{c}c$-pair, produced in higher–twists processes with participation of more than one valence quark of a hadron, is longer, than that of sea quark pairs and these $\bar{c}c$-quarks must carry a significant part of the primary hadron momentum, i.e. to have increased values of x_F.

Since intrinsic $\bar{c}c$-pairs with a certain probability can be brought on mass shell through a "soft" hadron–nuclear collision, whose cross section has a dependence of $A^{2/3}$, and a contribution of the intrinsic charm in the total cross section of J/Ψ-particle production grows with an increase of their x_F and decrease of p_t, this mechanism, as it has been shown in Ref.[20], could lead to the observed x_F- and p_t-dependences of the parameter α. Furthermore, because the intrinsic $\bar{c}, c$-quarks have rapidities, close to those of valence quarks of an projectile, they should demonstrate an increased probability of recombination in a colourless hadron with a comoving projectile valence quark (anti–quark). This would give rise to longitudinal momentum of such a hadron. In Ref.[18] it was demonstrated, that in order to describe the leading and non leading charm hadron asymmetry, observed in the experiments WA82 and E769, about half of intrinsic $\bar{c}, c$-quarks must recombine with a projectile valence quark and the rest of them just fragment.

An indication of intrinsic charm presence in a nucleon was independently obtained in EM–Collaboration experiment on muon–nucleon scattering, where at $x_F \geq 0.15$, $Q^2 \leq$ 40 GeV a marked exceeding of charm production in comparison with the predictions of the photon–gluon fusion model [21] was observed. A theoretical analysis of these data showed, that a probability of the nucleon wave function to exist in the state with an intrinsic charm is (0.3–0.5)% [22].

By assuming the lower limit of this estimation, in Ref.[18] a conclusion was made, that in πN-interactions the cross section of the charm production at $x_F > 0$ through the mechanism of intrinsic charm release at the energies of CERN and FNAL experiments was about 0.5 μb, which corresponded only to 5% of the total cross section $\sigma_t(\bar{c}c)$. This value is within the limits of the parameter α measurement error bars in the last experiments on the study of "open" charm production. This fact could explain the absence in the results of these experiments of the expected effect of this mechanism on α.

However, this point of view is not widely accepted. For example, in Ref.[23] an attempt was made to explain the $\alpha(x_F)$-dependence, registered in the experiment [10], without using the intrinsic charm hypothesis.

Though the expected contribution of the mechanism of intrinsic charm release in the total cross section of the charm hadroproduction cannot be big, nonetheless an elucidation of the problem of its existence is of the fundamental importance for the charm physics. In experiments at high energy this mechanism, as it was already demonstrated in Ref.[9], in the view of kinematics can hardly be distinguishable from the charm diffraction production, which to-date arouses a strong theoretical interest. In accordance with contemporary theoretical ideas [24], heavy quarks at diffraction must be produced in subprocesses of hard scattering of a parton of an incident hadron with a pomeron constituent (presumably gluon). Therefore, the process of the heavy quark diffractive production can be considered as one of a few sources of information the about a pomeron structure. In the case of intrinsic heavy quark existing, this mechanism can essentially distort the characteristics of the samples of c- and b-particles, detected in the experiments on their diffractive production.

Thus, at present an experimental verification of the intrinsic charm hypothesis appears to be one of the most urgent problems. It is of particular importance to compare the predictions of the model formulated in Ref.[18] with the A-dependence of charm x_F-spectra, which at CERN and FNAL energies requires a significant (by orders) enlargement of statistics. However, the cross section of $\bar{c}c$-pair production in hard QCD–subprocesses rapidly falls with energy decrease, while the charm production through the mechanism of the intrinsic charm release has a weak energy dependence, proper for the total cross section of hadron–hadron interactions [18], down to the kinematic limit. Hence, in investigations of the particles with "open" charm such a mechanism must more distinctly reveal itself in hadron beams with a momentum smaller than 100 GeV/c. In particular, in pN-interactions at 70 GeV/c ($\sqrt{s} = 11.8$ GeV) $\sigma_h(\bar{c}c)$ of hard subprocesses must be of 1 μb. Therefore, a contribution of intrinsic charm mechanism in the total cross section $\sigma_t(\bar{c}c)$ can reach 50%.

This allows one to consider a search in the charm hadroproduction at 70 GeV/c of the effects, related to the intrinsic charm release mechanism, and an estimation of the mechanism contribution as the main physical goal at the second stage of the experiment E–161.

2.1.2. Possibilities to determine a contribution of intrinsic charm by using an A-dependence of inclusive spectra of charm particles

In order to search for an effect of intrinsic charm in inclusive x_F–spectra of charms in the reactions:

$$pA \to \bar{D}D + X, \tag{1}$$

$$pA \to \bar{D}\Lambda_c^+ + X, \tag{2}$$

$$pA \to D\bar{\Lambda}_c^+ + X, \tag{3}$$

$$pA \to \Lambda_c^+ \bar{\Lambda}_c^+ + X, \qquad (4)$$

it is proposed to use a special target of thin plates with different values of A : a plate of tungsten, W, and further thin semiconductor counters of Si and/or $GaAs$. In proton interactions with Si nuclei ($A = 28$) the cross section of hard processes, having the dependence $\sigma_h \sim A^{1.0}$, must increase 3.04-fold in comparison with the cross section, having the dependence $\sigma_s \sim A^{2/3}$, while for Ga and As nuclei ($A = 70$ and 75 respectively) this difference at average is 4.17, and for W nuclei ($A = 184$) it reaches 5.69.

Since, as shown above, a contribution of the intrinsic charm release mechanism must concentrate at large x_F and small p_t, a population of these regions in $p(Ga,\ As,\ W)$-interactions must be relatively smaller, than in pSi-interactions. This difference can be displayed in a deviation from the constant of the ratio:

$$R(x_F, p_t) = \frac{d^2\sigma_{Si}}{A_{Si} \cdot dx_F \cdot dp_t^2} \Big/ \frac{d^2\sigma_k}{A_k \cdot dx_F \cdot dp_t^2},$$

(where A_k – nuclei of As, Ga or W,) for charm $D^{\pm}$ and $\bar{D}^0, D^0$-mesons.

An estimation of this effect for protons with the momentum of 70 GeV/c was made in Ref.[25] on the basis of the model, described in Refs.[18,20]. In this model the hadronization of charm quarks, produced as a result of the intrinsic charm release, takes place owing to both their usual fragmentation and recombination with projectile valence quarks, giving the leading component.

In Fig.3a the ratios $R(x_F)$ of charm D-meson $d\sigma/dx_F$-cross sections per nucleon in pSi and pW-interactions are shown. The ratios were calculated in the assumption, that $\sigma_{intr.}(\bar{c}c)$ for $x_F > 0$ in nucleon – nucleon interactions makes 0.35 μb or 0.7 μb. In Fig.3b the analogous distributions for $\bar{D}$-mesons are given. As follows from these Figures, the effect of the intrinsic charm release mechanism is much stronger in the case of $\bar{D}$-mesons, which x_F-distribution has the leading component. In accordance with similar calculations, in order to discover the effect of the intrinsic charm mechanism samples of a thousand $\bar{D}$-mesons for Si- and W-target are sufficient. The statistics of 3 thousand $\bar{D}$-mesons in a sample for each target, to which the error bars, given in Fig.3, correspond, allows one to estimate the contribution of the instrinsic charm release mechanism to the charm yield with the accuracy up to 0.3 μb.

This contribution should be rather distinct also in Λ_c^+-baryon $R(x_F)$-distribution, the results of which simulation are given in Fig.4a. The error bars on the curves in Fig.4 conform to the statistics of 3 thousand Λ_c^+-baryons for each target. On the other hand, as follows from Fig.4b, the intrinsic charm contribution leads only to an unsignificant A-dependence of x_F-distributions of "non-leading" $\bar{\Lambda}_c^+$-baryons.

The presence of the intrinsic charm contribution can be also determined by using the value of the asymmetry parameter $A(x_F)$, described above. The estimation of this effect, made in the framework of the model referred above, for D-mesons and Λ_c-baryons gave $A_x = \int_0^1 A(x_F)dx_F$ being 0.096 and 0.26 respectively for pSi-interactions, as well as 0.057 and 0.17 respectively for pW-interactions. A measurement of $d\sigma/dx_F$-distributions of D-mesons for 3 different nuclear targets also allows one to determine x_F-dependence of the

parameter α. A determination of a x_F-dependence of α by using Λ_c^+-baryon spectra, for which no such data have been obtained, so far is also of great interest [18].

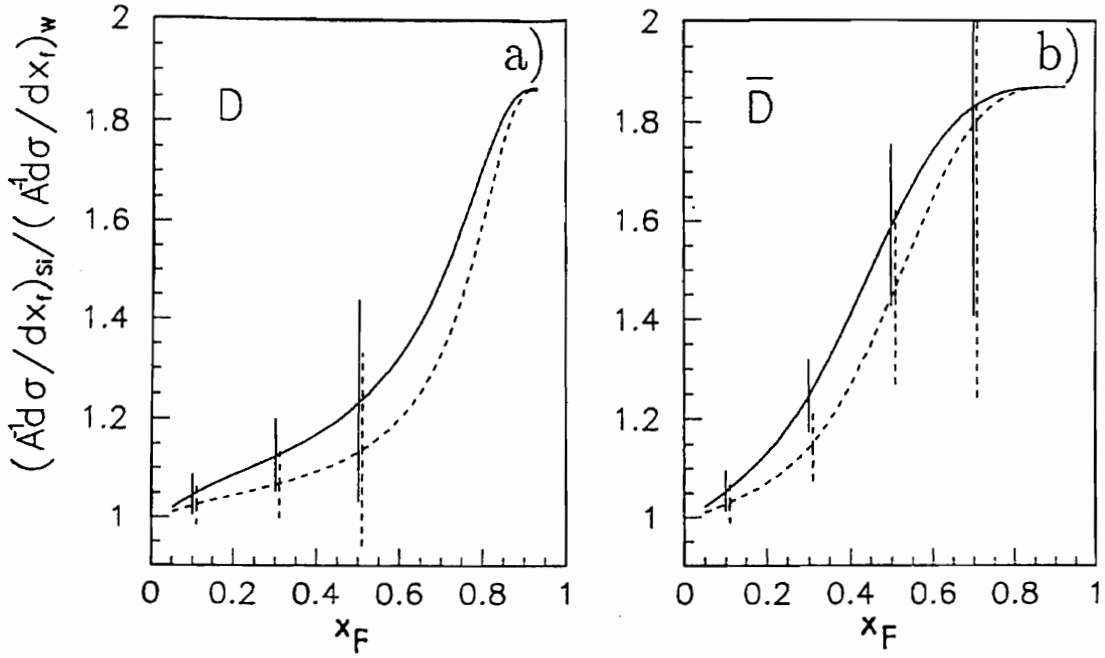

Fig. 3. Ratios of normalized to a nucleon x_F-distributions of the charms, produced in pSi and pW-interactions for: a) D-mesons; b) $\bar{D}$-mesons. Solid line $\sigma_{intr.x>0}(\bar{c}c) = 0.7\ \mu b$; dashed line –0.35 μb.

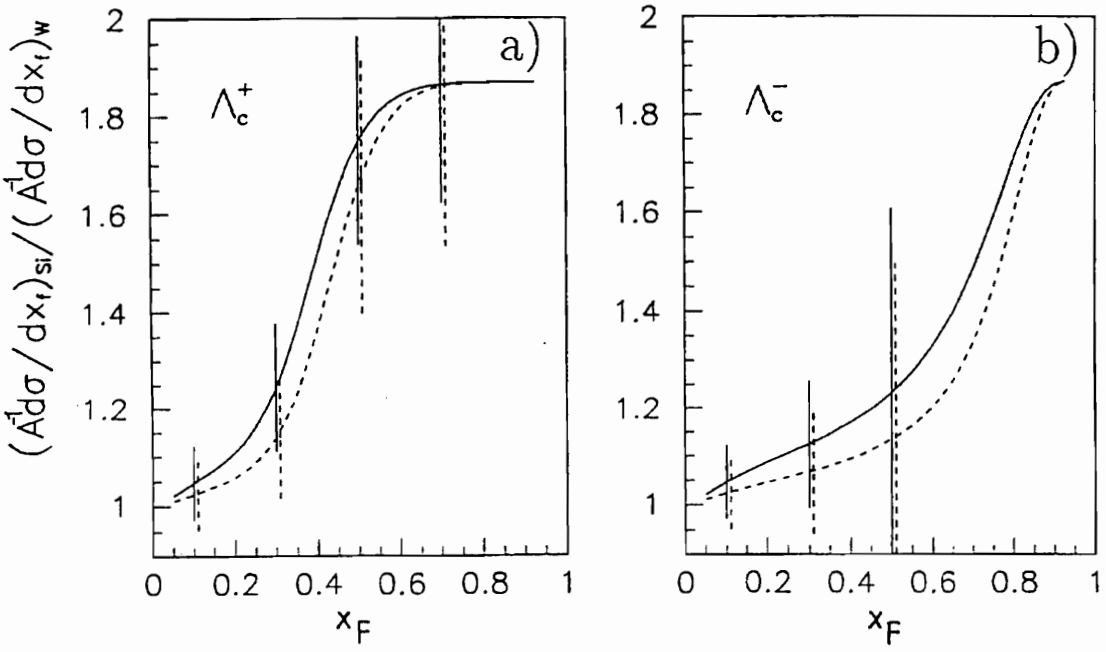

Fig. 4. Similar ratios for a) Λ_c^+-baryons; b) $\bar{\Lambda}_c^+$- baryons.

Another characteristic variable, which in the presence of the intrinsic charm mechanism contribution must vary with the change of the atomic number of the nucleus of a target, is the mean transverse momentum of charms in the region of large x_F.

Since $< p_t >_{hc}$ of the charms, produced in processes of hard scattering of partons, is about 3 times higher, this value for hadrons in "soft" interactions, and $< p_t >_{ic}$ of the charms, produced through the intrinsic charm release mechanism, should be close to the last one, the contribution of this mechanism must cause a decrease of $< p_t >_c$ in the region of large x_F, where this contribution is maximal. Fig.5a shows x_F-distributions of $< p_t >_c$ for $\bar{D}$-mesons produced in pSi- and pW-interactions. The distributions were calculated in the assumption, that $\sigma_{intr}(\bar{c}c)$ in pN-interactions is 0.7 μb. Making these calculations, it was supposed, that $< p_t >_{hc}$= 1.0 GeV/c, $< p_t >_{ic}$= 0.5 GeV/c, and that they do not depend on charm x_F. A rapid decrease of $< p_t >$ with x_F because of the increasing contribution of intrinsic charm is seen. As the results of simulation with PYTHIA program made with the charm quark fragmentation function in the form of a δ-function (the dotted curve on Fig.5a) have shown, this effect is absent in the case of the charm hadroproduction only in subprocesses of hard scattering of partons. In Fig.5b similar distributions for Λ_c^+-baryons are demonstrated. The statistical errors in both Figures conform to 3 thousand particles for every target.

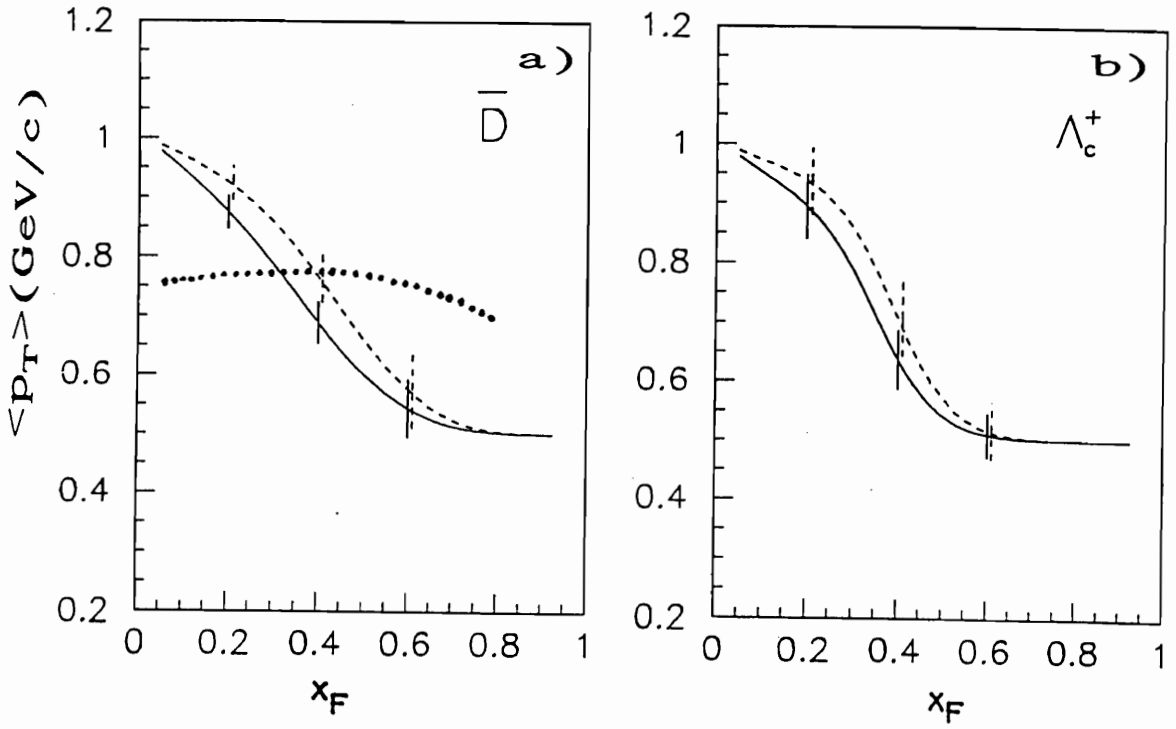

Fig. 5. X_F-dependence of $< p_t >_c$ of the charm hadrons, produced on Si nuclei (the solid line) and on W nuclei (the dashed line) for a) $\bar{D}$-mesons; b) Λ_c^+-baryons. The dotted curve in a) is the results of the PYTHIA calculations.

2.1.3. Influence of intrinsic charm on x_F–dependence of correlations between the transverse momenta of two charms

Calculations of correlations between the transverse momenta of heavy quarks were made in the context of perturbative QCD with the accuracy to the next–to–leading order processes [26]. They showed that in the transverse momenta plane the charms, produced in processes of hard scattering of partons, must be emitted presumably in the opposite directions. As a result, the distribution over the azimuthal angle φ between p_t of two charms must have a clear peak at $\varphi = 180^0$. The investigations, carried out in a number of experiments at CERN and FNAL energies [27,28], confirmed the presence of the effect. So, the experiment WA92 revealed that in $\pi^- A$-interactions at 350 GeV/c [29] the distribution over angle φ in $D\bar{D}$-meson pairs had the asymmetry parameter

$$A_\varphi = \frac{N_{\varphi>90^0} - N_{\varphi<90^0}}{N_{\varphi>90^0} + N_{\varphi<90^0}} = 0,73,$$

i.e. for 86% pairs the angle φ exceeds 90^0. It is shown, that the experimental φ-distribution agrees well with the calculations, made by using the perturbative QCD with the next–to–leading order corrections in the assumption, that the colliding partons have $< p_t^2 > \simeq 0,3$ (GeV/c)^2.

For the charm pairs, produced due to the intrinsic charm release mechanism, this effect must be absent, since in "soft" interactions an effect of local compensation of the transverse momentum is not observed [30] and the azimuthal asymmetry is small (~ 0.1). Hence, the contribution of this mechanism must lead to x_F-dependence of the parameter A_φ, which will be the most visible in the subsample, obtained with the lightest nuclei (in our case, Si nuclei), where a relative contribution of the intrinsic charm must be the greatest.

Since at $\sqrt{s} \leq 12$ GeV charms are produced presumably through the channel $pA \to \bar{D}\Lambda_c^+ + X$, it is of interest also to investigate azimuthal correlations between the charm baryon and charm meson.

Another way to reveal an intrinsic charm contribution is to study the dependence of $< p_t >$ of a charm on $< p_t >$ of another charm in various x_F-intervals of one of them.

A presence of large negative correlations between p_t of the charms, produced in hard subprocesses, must lead also to a large value of their invariant mass $M(\bar{c}c)$. For the charm particles produced by intrinsic $\bar{c}c$-pairs $M(\bar{c}c)$ must be significantly smaller.

2.2. Study of nonleptonic decays of charm baryons

By this time a considerable progress has been achieved in theoretical and experimental investigations of charm meson decays [31,32]. Since the largest fraction of the cross sections $\sigma_t(\bar{c}c)$ in hadron – hadron interactions at high energies is realized via final states $[(\bar{D}D) + X]$, a considerable statistics has been already collected for various decay modes of D- and D_s-mesons [33] in CERN and FNAL fixed target experiments, as well as in experiments at intersecting e^-e^+-rings.

On the other hand the data on charm baryon decays have been much scarcer so far and a theoretical description of these processes is still far from completion [34].

Though the total cross section $\sigma_t(\bar{c}c)$ in pp-interactions at 70 GeV/c must be about by an order smaller, then in the experiments conducted in the momenta range 300 – 500 GeV/c, nonetheless according to theoretical estimations, its greater part is realized as the final state (charmed baryon + anti-charmed meson). Besides, if the estimations of intrinsic charm contribution, obtained in Ref.[19], are confirmed, a production of Λ_c^+-baryons in the proposed experiment will be comparable with their production in the experiments at higher energies. On the other hand, a smaller multiplicity of the charged, particles in pp-interactions at 70 GeV/c and the absence of a very narrow cone of particles from the fragmentation of the incident hadron must facilitate an identification of Λ_c^+-baryon decay products and to make the proposed experiment competitive with the ones on the study of Λ_c^+-baryon decays at higher energies.

At present nonleptonic exclusive channels of charm baryon decay attract a special interest. As it is known, nonleptonic decays of Λ_c^+-baryon can be caused by the weak decay of a charm quark and by the process of the W-meson exchange, whose Feynman diagrams are given in Fig.6. However, methods of calculations of Λ_c^+-baryon nonleptonic decay probability are still under development. In order to calculate probabilities of a large number of decay channels including multiparticle ones hitherto phenomenological approaches based on statistical methods were used [35].

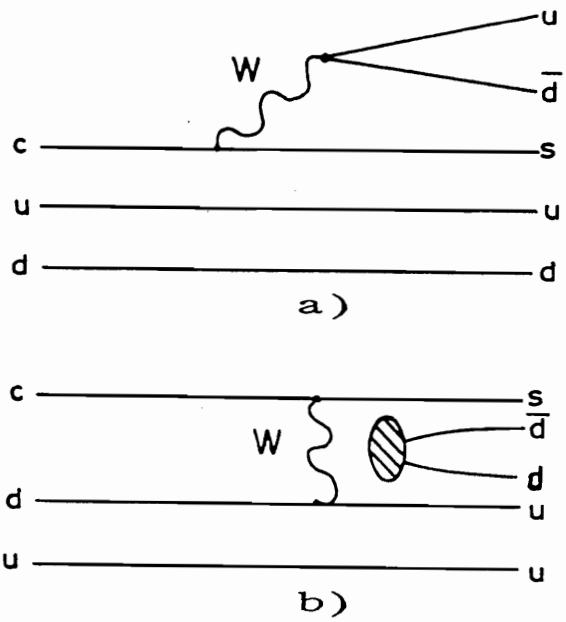

Fig. 6. Feynman diagrams for Λ_c^+-baryon decays, corresponding: a) to weak decay of c-quark; b) to exchange by W-boson.

Recently developed methods of two–particle and quasi–two–particle decay calculations offer real opportunities to verify a number of Standard Model (SM) theses. These methods use quark diagrams and are based on the algebra of currents as well as on the symmetry requirements. According to them the amplitudes are classified correspondingly to the quantum number change and their transfer in nonleptonic decays.

In a pioneer work on this problem Körner et al. [36] considered a total set of possible quark diagrams with a quark decay and a W-exchange. Calculating amplitudes in the approximation of the spectator quark model, they used for quarks the $SU(2)_W$ spin wave functions. More accurate results of the calculations with the use of this model are given in Ref.[37].

Ref.[38] shows, that to the decay $B_c \to BP$ (where P is a pseudoscalar meson) a more general factorization approach developed to describe the charm D-meson decays [31] can be applied, in which one of quark currents directly generates a pseudoscalar

meson. However, this approach is applicable only in the "soft mesons" limit, and an additional estimation of non-factorizable contributions appears to be required here. It is also elucidated that diagrams with a W-exchange are not prevailing in charm baryon decays, in contrast to strange hyperon decays.

Considerable results have been recently obtained on the basis of the pole model, in which the decay amplitude of a charm baryon is approximated by contributions of the baryon and meson poles, including resonances and continuum states [39]. However, in this model the calculation results are also still ambiguous and strongly depend on suppositions about quark wave functions (MIT bag model was used in Ref.[39] for their estimation), on the method of the vertex constant calculations etc.

A comparative analysis of the results obtained which uses the algebra of current and the pole model was carried out in Ref.[40], where also an attempt of their unification was undertaken.

In Table 1 the experimental results on some branching ratios (in %) of Λ_c^+-baryon, compared to various theoretical estimations, are given. It is seen, that among them a large difference still exists, and as Ref.[40] emphasizes only new precision experimental data will allow one to give the preference to one of the existing theoretical approaches.

As will be shown in Sect.4.2. a configuration of the SVD set-up allows one to quite effectively detect both main modes of Λ_c^+-baryon decay and still poorly studied modes, such as $\Lambda_c^+ \to \Lambda^0\rho^+$, $\Lambda_c^+ \to \Sigma^+\rho^0$.

Table 1

	[39]	[37]	[40]	exper.
$\Lambda_c^+ \to p\bar{K}^0$	1.2	2.6	1.9	2.1 ± 0.4
$\to \Lambda\pi^+$	0.87	1.0	0.59	0.58 ± 0.16
$\to \Lambda\rho^+$	$2.3 \div 2.6$	18.2	0.51	< 4
$\to p\bar{K}^{0*}$	$1.8 \div 3.3$	2.9	2.27	1.6 ± 0.4
$\to \Sigma^+\pi^0$	0.72	0.31	0.43	0.87 ± 0.22
$\to \Sigma^+\rho^0$	$0.03 \div 0.19$	3.0	0.53	< 1.2
$\to \Sigma^0\rho^+$	$0.03 \div 0.19$	-	-	-
$\to p\varphi$	0.19	0.20	0.1	0.13 ± 0.09

A reconstruction of two–particle decays of Λ_c^+-baryon also allows one to determine the asymmetry parameter, α_c, of a Λ_c^+-baryon decay by which one can estimate the parity violation amplitudes values. In the decay $\Lambda_c^+ \to \Lambda^0(\to p\pi^-) + \pi^+$ the cascade decay $\Lambda^0 \to p\pi^-$ can serve as an analyzer of the longitudinal polarization of a daughter Λ^0-hyperon, which is directly determined by the parameter α_c. The first results of α_c measurements for this decay within the limits of large error bars coincide with the model predictions, which take into account a violation of SU(4) symmetry [40]. A more complicated picture appears at the decay $\Lambda_c^+ \to \Lambda^0(\to p\pi^-) + \rho^+(\to \pi^+\pi^0)$, where the longitudinal polarization of Λ^0-hyperon is determined by the contribution of the amplitude with CP–violation and by the effect of interactions in the final state. In SM the first contribution must be rather small and for its isolation cascade decays of Λ_c^+ and $\bar{\Lambda}_c^+$-baryons [34] are to be compared.

3. CONFIGURATION OF THE SVD SET-UP FOR THE 2ND STAGE OF THE EXPERIMENT

In order to solve the problems, enumerated above, an experimental set-up is needed, which would allow one to restore the kinematic characteristics of charms in a wide range of their x_F and p_t. As Ref.[1] shows, such possibilities from the very beginning were foreseen in the SVD project.

However, to fulfill the second stage of the experiment E–161, the SVD set-up must be upgraded and supplemented with a number of new detectors.

An outline of the upgraded set-up is given in Fig.7. A large aperture magnetic spectrometer with multiwire proportional chambers (MWPC), as well as the detector of γ-quanta, consisting of Čerenkov full absorption counters, manufactured and tested at the first stage of E–161, serve as a base of the set-up.

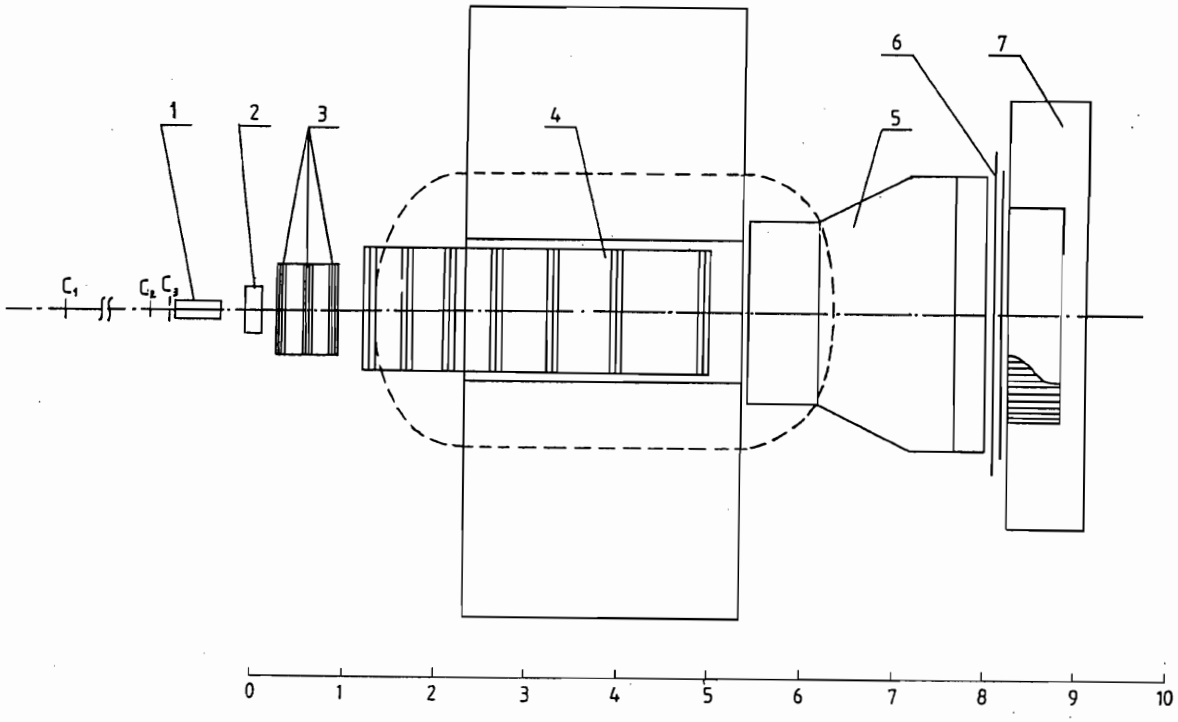

Fig. 7. Schematic view of the SVD set-up for the second stage of the experiment E-161: 1 – precision vertex detector; 2 – block of minidrift tubes; 3 – forward block of 1 m MWPC; 4 – central block of MWPC; 5 – threshold Čerenkov counter; 6 – scintillation hodoscopes; 7 – detector of $\gamma-$quanta.

For the second stage of the experiment the following new detectors are to be prepared:

– the precision fast operating vertex detector on the basis of microstrip silicon detectors;

– the block of mini-drift tubes containing 8 planes;

– the multicell threshold Čerenkov counter.

Besides, a new trigger electronics as well as a system of data acquisition and presentation with a modern fast local communication network and with the new generation of on-line computers, should be designed and manufactured.

A more detailed description of the main detectors and systems of the SVD is given below.

3.1. The precision vertex detector

A considerable progress in the investigation of charm hadroproduction was achieved for the last years due to a development of the technique of precision vertex detectors (PVD), based on the electronic method, as well as to an introduction of powerful processors, capable of fast handling large samples of experimental data. This technique allows one to estimate a secondary track impact parameter with respect to the primary vertex for the selection of events with shortliving particle decays in the real time of the experiment, as well as to restore the vertices of these decays. Additionally, targets with various atomic numbers A may be easily used inside of the PVD.

In the new generation of fixed target experiments on a study of heavy quark photo- and hadroproduction at CERN and FNAL, complicated PVDs containing a large number of microstrip silicon detectors (MSD) with a few tens of thousands of channels [7,41,42], are used. The amount of completely restored decays of charms in the experiments, carried out at present, already reaches the level of 10^5, which allows one to go on the detailed investigation of the charm quark hadroproduction dynamics and mechanisms of the quark decay. Since a value of the impact parameter $\delta \approx c\tau$ does not practically depend on the momentum of a decaying charm, the PVD technique can be efficiently used for an improvement of the signal–to–noise ratio in the studies of charm hadroproduction at the near-threshold energy.

Therefore for a realization of the second stage of the experiment E–161 it is proposed to use a fast operating PVD, which structure is optimized for the range of energies under investigations.

The main functions of the PVD will be as follows:

– at the level of event selection the PVD must provide accurate measurements of the interaction point as well as of the coordinates on the trajectories of the primary charged particle and of the secondary ones; these measurements would allow one to establish a fact of the primary particle interaction in a target and the presence of secondary vertices, close to the primary one;

– at the level of geometrical reconstruction of tracks the counts from the PVD detectors must guarantee a high two-track separation for the charged particles emitted at small angles;

– at the level of the event topology restoration the data obtained using the PVD must provide a reconstruction of the secondary vertices, located at a distance less than 5 mm from the primary interaction, as well as the connection of the "tertiary" tracks to secondary vertices.

To fulfill these functions the PVD will include the following elements schematically shown in Fig.8:

– beam telescope T_1 consisting of 3 pairs of MSD with an orthogonal orientation of microstrips, (MSD_{1-6} in Fig.8), which measure the vertical (x) and horizontal (y) coordinates of a beam particle; the dimensions of these MSDS and the values of their pitches are given in Table 2;

– active target (AT) of a tungstic foil and 3–4 thin semiconductor counters with the working surface $\sim 1,0$ cm^2, which are placed at 2 mm apart; the first (relative to beam direction) counter, placed before the foil is made of Si, while the ones situated behind the foil are made of $GaAs$ or Si;

– vertex telescope T_2, including a charge coupling device (CCD), three X,Y pairs of MSD, belonging to the trigger system and quadruplet $UYVX$ (where U and V are inclined relative to the vertical line at the angles of $\pm 10.5^0$), which functionally is part of the SVD magnetic spectrometer track system. The parameters of MSDs are given in Table 2. The CCD with the sensitive area of 9.0×6.7 mm^2 possesses 17×17 μm^2 pixels.

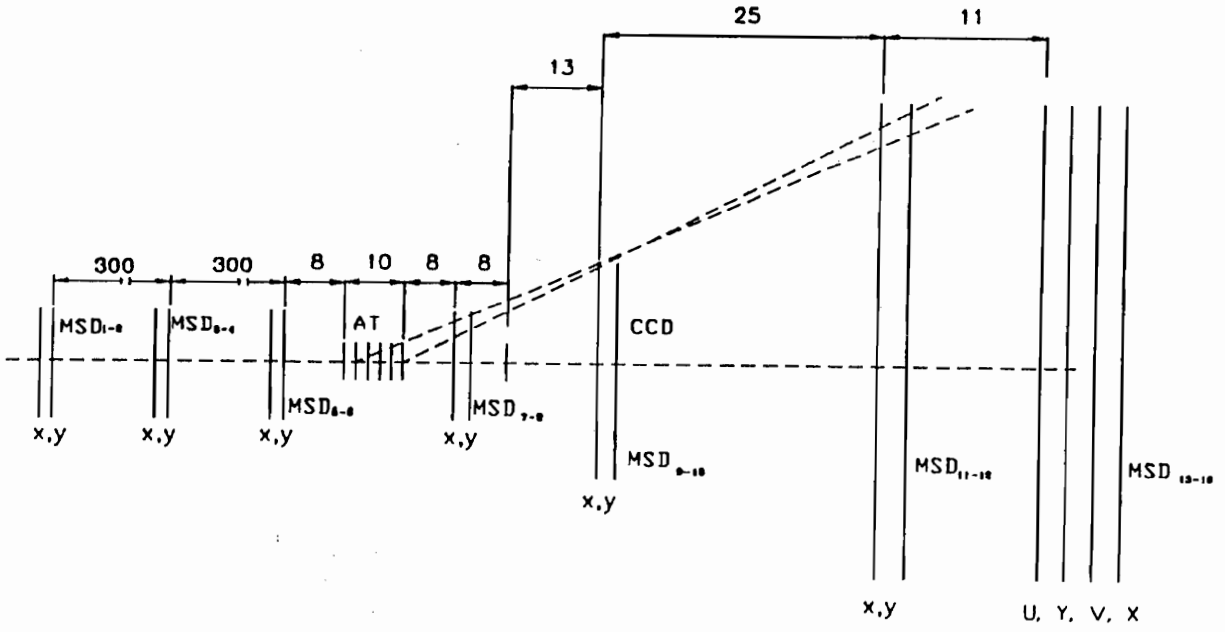

Fig. 8. Scheme of PVD.

A detailed simulation of the PVD design with the purpose of its optimization for the charm event selection showed that at a beam particle momentum less than 70 GeV/c the telescope T_2 must have sufficiently small distances between the pairs of MSD, included in the trigger part, as well as be placed close to AT.

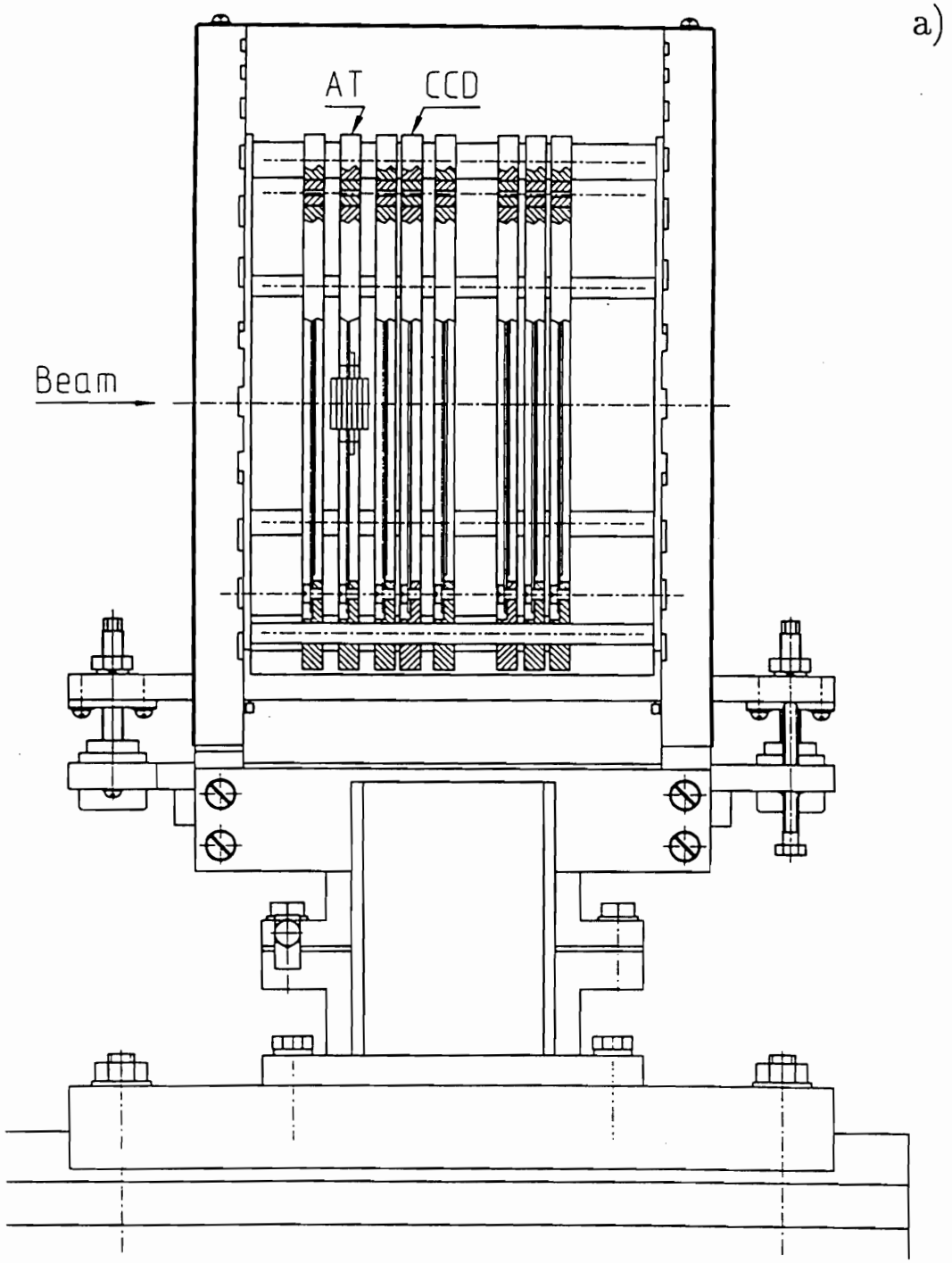

Fig. 9. General view of the PVD mechanics with the readout electronics (project): a) side view; b) front view.

b)

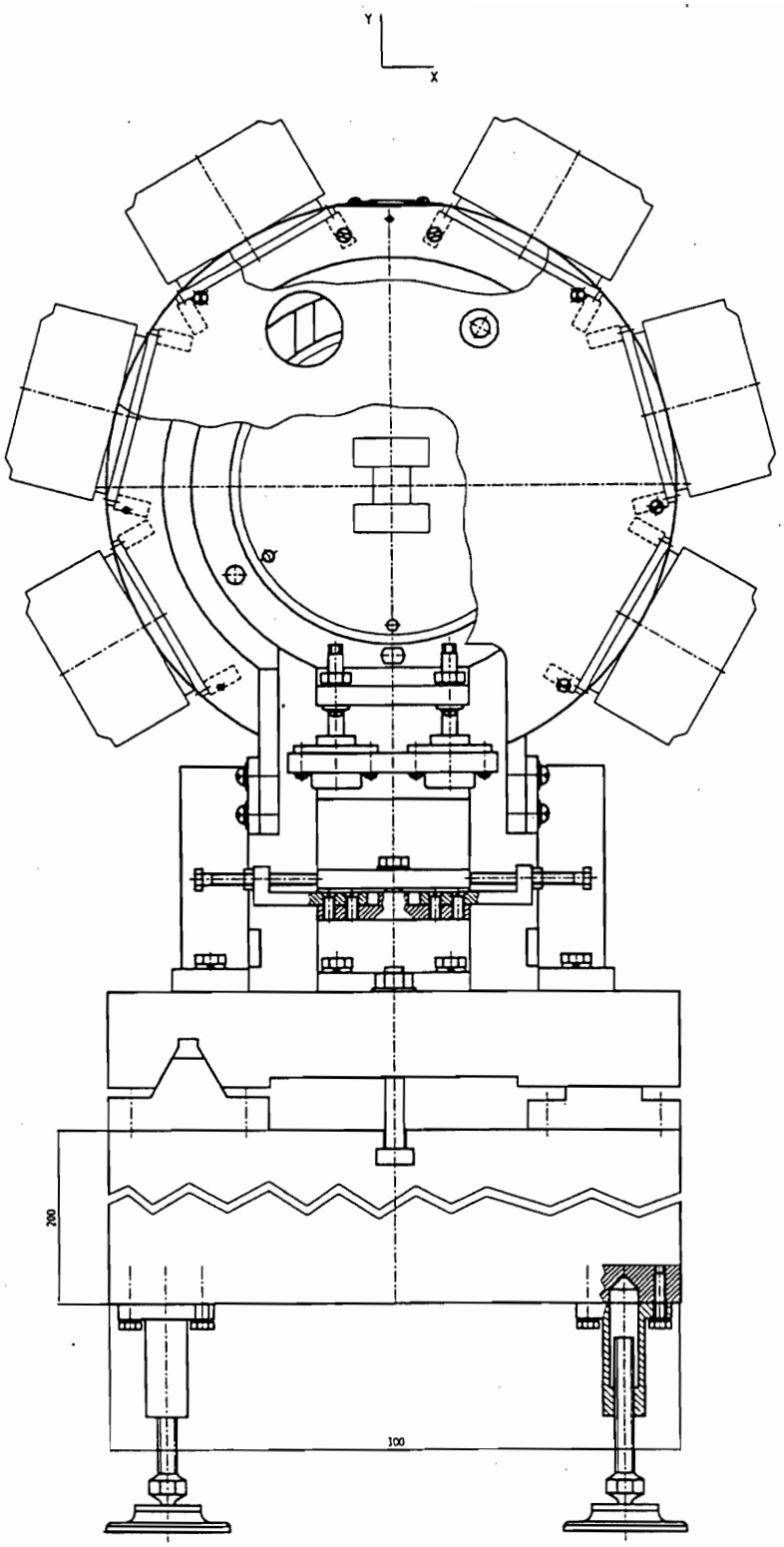

Table 2

N MSD	Dimension, mm^2	Pitch, μm	Strip orientation	Number of strips	Type of preamplifier
1,2	5×5	25	X,Y	192×2	AMPLEX
3,4	5×5	25	X,Y	192×2	AMPLEX
5,6	5×5	25	X,Y	192×2	AMPLEX
7,8	16×16	25	X,Y	640×2	AMPLEX
9,10	32×32	50	X,Y	640×2	AMPLEX
11,12	58×58	50	X,Y	1152×2	AMPLEX
13,14	58×58	100	U,Y	576×2	VIKING
15,16	58×58	100	V,X	576×2	VIKING

In order to simplify the tasks of precision adjustment of AT and MSD in a common coordinate system, $MSD_{5,6}$, AT and MSD_{7-16} are fastened in a common hard mechanical frame which is adjusted as integral part relative to the coordinate system of SVD.

A general view of this construction is given in Fig.9. It is assembled of aluminium discs of 270 mm in diameter and 8 mm thick, having in the centre the openings of 200 mm in diameter. On the edges of the opening from each side of the disc the plates with MSD are fastened. Two MSDs, fastened at a disc, form X,Y-pair, with the exception of the two last pairs, being part of the quadruplet.

An orthogonality of the strips of each MSD pair is guaranteed by their adjustment at a UIM–21 microscope relative to repers marked on a disc. The distances between the discs are regulated with precision spacers, and the accuracy of their reciprocal position in the azimuthal plane is provided due to an accurate manufacturing of the holes at the outer disc edges and of rods, fastening discs. AT is also fastened in the centre of such a disc, which provides a stability of a relative position of the main PVD components. This central PVD block is mounted on a optical bench (usually for such purposes a marble bench is used), on which on separate supports the two remaining MSD pairs of T_1 are also fastened. For an accurate determination of the primary particle angles the distance between $MSD_{1,2}$ and $MSD_{5,6}$ must be about 50 cm.

The PVD preamplifiers are located in an immediate proximity to them on special ring–like bearings, fastened directly on the carrying bench of the assemblage.

The semiconductor counters of AT are equipped with low-noise amplifiers, designed for a considerable capacity of the detectors. Signals from the amplifiers are transferred to fast ADCs. The results of digitization are transmitted to the fast processor of the trigger system $L1$.

All the MSD of T_1 and MSD_{7-12} of T_2, the information from which is used at the second level trigger ($L2$) can be equipped with chips of the AMPLEX type with 16 channels per chip, having a charge amplifier, a shaping amplifier, a track and hold stage and an analog multiplexer. On the other hand MSD_{13-16}, included in the track part of the system, can have microschemes of the AMPLEX or VIKING types with 128 channels.

The charge signals held by AMPLEX are read out serially by CAMAC encoding modules with 8 bit ADC.

In a single CAMAC module 8 ADC channels are supposed to be housed. A generator of controle signals will be also manufactured as a module of CAMAC 1M.

The use of ADC in readout channels allows for efficient selecting signals from microstrips, hitted by charged particles, among noise signals, as well as for processing clasters.

3.2. The block of minidrift tubes

In order to connect tracks of charged particles in PVD with the tracks, reconstructed in MWPCs of the magnetic spectrometer, an additional block of minidrift tubes is introduced between them.

The last one is a system of cylindrical thin wall counters (tubes) assembled in eight two–layer planar modules. Each counter is manufactured from 50 μm thick capton film; the internal surface of a tube is covered with a layer of graphite, having the resistivity of 50 $k\Omega$/square. The tube diameter is 10 mm.

The anode is a wire of 30 μm in diameter. In the plane the tubes are located at 15 mm distance between the centers. The second plane of tubes is 7.5 mm distant from the first one (Fig.10a). In order to increase the position measurement precision a cathode signal readout will be used. Therefore the counters will actually operate as proportional gas tubes. For this purpose the external surface of the tubes is covered by a metalized coating in a form of rings (Fig.10b) with a width of 5 mm. The distance between the rings is 1.5 mm. All the rings having the same position at a tube are electrically connected with each other by cathode readout buses passing perpendicularly to the anode wires (Fig.10). As a whole each module consists of 65 tubes of 520 mm in length, covers the area of 520×500 mm^2 and contains 80 lines of cathode readout. The total system consists of 8 modules, organized in two quadruplets $UYVX$. The complete system includes 520 tubes and 640 channels of the cathode readout. The working gas mixture is argon + methane (60% and 40% respectively). A working voltage applied to wires is about 3 kV. The signal

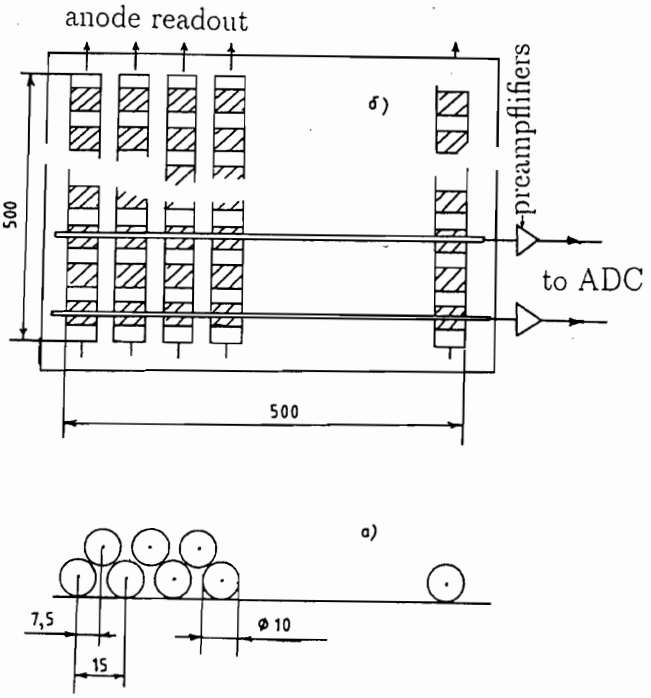

Fig. 10. Scheme of the minidrift tubes location in a module.

from a cathode readout line after an amplifier goes to 8-bit fast ADC. The coordinate along a tube is determined by weighing the amplitudes from 3–5 adjacent channels. The accuracy of the coordinate determination is about 150 μm [43].

The electronics of the cathode information readout also includes the following elements:

– block for a fast finding of 3–5 adjacent rings with induced signals, one per each module;

– buffer memory for a storage of the information from the groups of adjacent channels and of their addresses.

For the counters a readout of the anode signal is possible, which can be used in $L1$ trigger. Being equipped with additional TDC modules, the microdrift tubes can simultaniously work in their standard mode.

3.3. The large aperture magnetic spectrometer

For measurements of secondary charged particles momenta the SVD includes the large aperture magnetic spectrometer with MWPCs. The spectrometer is manufactured on the basis of the electromagnet MC-7A, which is 3 m long at the poles (along the beam direction) and has an aperture of 1.8 m (width)× 1.3 m (height). At the primary particle momentum below 70 GeV/c the magnet operates at a reduced current ($I = 4\ kA$) and has in the working volume a rather homogeneous field of about 1.18 T.

The coils, which are bent up and down, stick out in front of the magnet and behind it (along the beam direction). This creates a strong stray magnetic field, which at 1.5 m distance from the magnet yoke has the value 0.08 T.

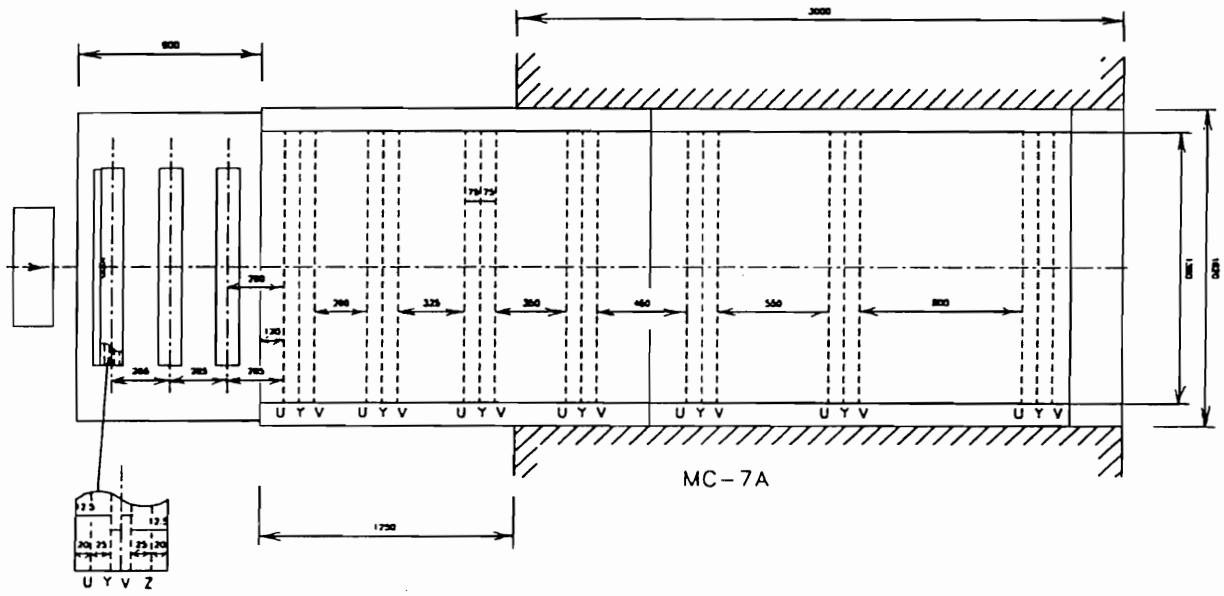

Fig. 11. Scheme of the location of MWPCs of the magnetic spectrometer.

The location of the magnetic spectrometer MWPCs is shown in Fig.11. From the functional point of view the magnetic spectrometer of SVD is of two stages. Its first stage

is formed by a front block of 12 MWPC, which is located before the magnet in its stray field. The block is used, in particular, to measure small momentum particles, emitted at large angles. The MWPCs with interwire distances of 2 mm and a sensitive area of 1.0 m^2 are joined into 3 quadruplets with wire orientation $UYVX$. A total number of signal anode wires in these chambers amount to 5424. This block is taken without changes from the first stage of the experiment. A central block located between the magnet poles consists of MWPCs with interwire distances of 2 mm and a sensitive area of 1.0×1.5 m^2. The following changes are proposed for this block structure: the first duplets UY and VY, used at the first stage, should be developed to triplets UYV by using the available spare MPWC's. The other 15 chambers of the central block remain grouped in five triplets UYV. From the functional point of view all the chambers of the central block present the second stage of the spectrometer and provide the measurements of particles momenta, emitted in the forward cone. On the whole they will contain 13504 signal anode wires. Constructively, the central block of MWPCs consists of two parts, each being a mobile metallic carriage, on which MWPCs are fastened. These are successively rolled into the magnet aperture from behind. The design of the magnetic spectrometer chambers and their characteristics are described in more details in Ref.[44].

With the exception for three X-planes of the front block, which are included in the trigger system and have a special system of information readout, the rest of chamber planes are equipped with fast amplifiers, located on the chamber frames. The signals from them are transmitted by 52 m long twisted pairs to readout electronics placed in CAMAC crates. Each separate module of readout electronics receives the data from 64 channels, so the electronics for one plane of MWPC is put in one crate. The magnetic spectrometer readout electronics includes 5 branches, containing 30 crates of CAMAC, which are governed by the control crate. The control crate is connected with the magnetic spectrometer computer, which in turn is linked through a local network to the central computer of the SVD set-up. After obtaining the appropriately timed trigger strobe signal the crate controllers of the readout electronics search for hitted wires in each crate (chamber) for 10 μs and write down their numbers in intermediate buffers. A readout of intermediate buffers is made by computer serially through the central crate with the maximal rate of 2 μs/word. A detailed description of the readout electronics of the magnetic spectrometer is given in Ref.[45].

The described organization of the spectrometer MWPCs allows one to use for the processing of the data, obtained from them, the program of the geometrical reconstruction TRIDENT [46], developed for the Ω-spectrometer at CERN. This program was in the appropriate way modified for the SVD set-up geometry, in which interactions take place in the precision vertex detector, located outside the magnet. After an adjustment of TRIDENT for the magnetic spectrometer of the SVD with events from pp-interactions at 70 GeV/c, simulated using the PYTHIA event generator and GEANT, it is found, that in modeled events about 60% of all tracks of charged particles are reconstructed. In Fig.12 the total x_F-distribution of charged particles in simulated pp-interactions at 70 GeV/c, as well as the corresponding distribution of the particles, whose trajectories were reconstructed by TRIDENT, are shown. It was also found, that trajectories of the

both charged particle were restored more than in 50% of all the two–particles decays of modeled K_s^0-mesons and Λ^0-hyperons. The simulation showed, that without using the information from the vertex detector the accuracy of the momentum measurements in the ranges 1–3, 3–8, 8–13, 13–18, 18–28 and 28–70 GeV/c are 5.1%; 2.3%; 1.4%; 1.8%; 1.6% and 2.8% respectively. The introduction in the magnetic spectrometer track system of three additional quadruplets of detectors with precision measurements of charged particle trajectories (one formed by MSD_{13-16}, and two – by minidrift tubes), as well as the inclusion in the track reconstruction algorithm of TRIDENT program of information about straigt tracks, reconstructed in the PVD, will widen the spectrometer aperture and will allow one to determine more accurately the momenta of slow particles, emitted at large angles.

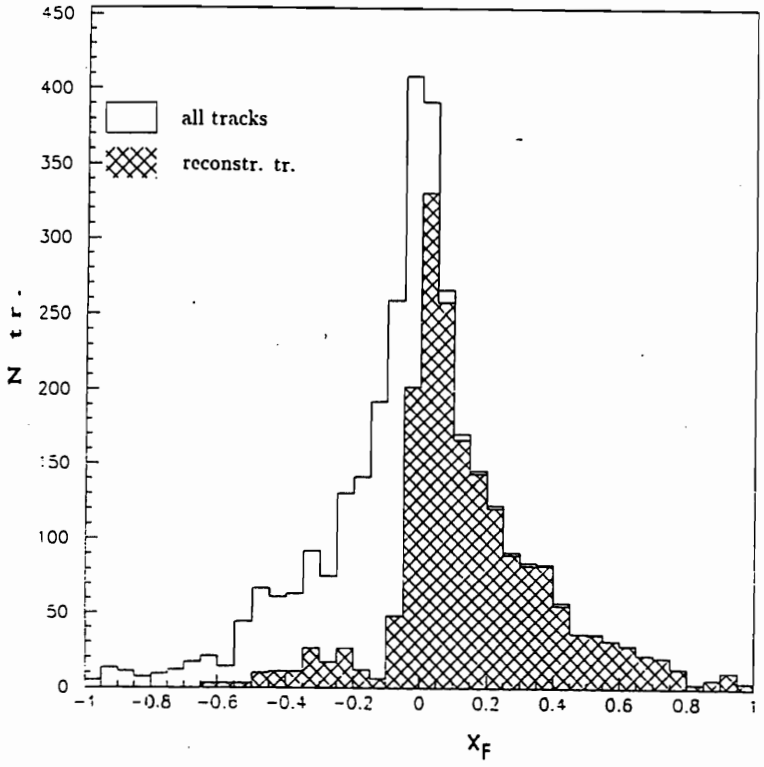

Fig. 12. x_F-distributions of the charged particles, simulated by the PYTHIA and distribution of the particles,which trajectories were reconstructed by TRIDENT.

In order to carry out this stage of the experiment, it is necessary to make a revision of the amplifiers, to acquire about 1.5 thousand UI-5 chips for equipping two new MWPCs with amplifiers and for replacing the broken ones, as well to prepare two new craters of readout electronics. It is also necessary to upgrade the gas distribution system and to acquire new sources of high voltage supply for MWPCs, which can be incorporated in the slow control system.

3.4. The multicell threshold Čerenkov counter

For an identification of charged particles the multicell threshold gas Čerenkov counter, placed between the magnet MC-7 and the scintillation hodoscope, will be used.

The counter consists of two sections 3 m long with an entrance aperture 177×130 cm. On the rear wall of the counter spherical mirrows are arranged in four rows of eight each. A mirror dimensions are 42×33 cm^2, with the curvature radius R=200 cm. The total surface, covered by the mirrors, is 265×155 cm^2 in a projection to the plane, perpendicular to the counter axis. The counter volume is looked through by 32 photomultipliers FEU–125 (with the cathode diameter of 140 mm) supplemented by Winston lenses. Near a photomultiplier a fast preamplifier is placed, a signal from which is transmitted by a coaxial cable to the entrance of a shaper amplifier and further, through a delay line to a strobed register. From the last one the signal is read out by a crate controller in a computer. The counter construction is schematically shown in Fig.13.

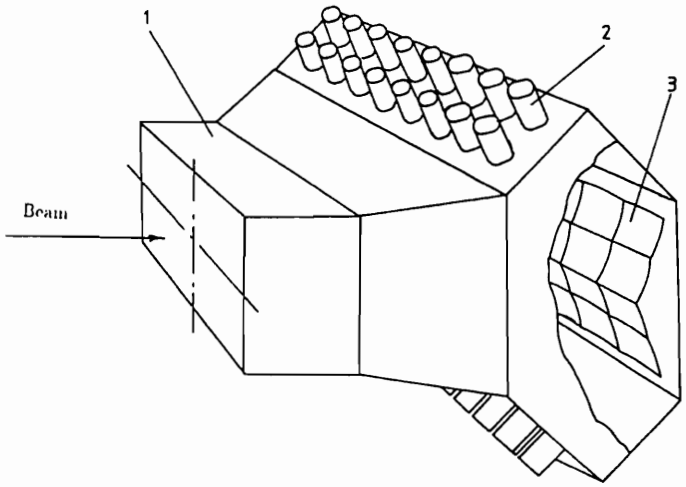

Fig. 13. General view of the threshold Čerenkov counter: 1 – segmented casing of the radiator; 2 – PM block with light – protective covering and magnetic screen; 3 – focusing mirrors.

When filled with argon under the atmospheric pressure and at the temperature of 20°C the Čerenkov counter provides the indentification of π-mesons in the range of momenta from 6 to 21 GeV/c with the efficiency of 98%, which allows in 50% cases for reliable separating D^0- and $\bar{D}^0$-mesons, registered in the spectrometer. Dimensions of the counter were optimized for simulated events by the use of the GEANT program. The position of the Čerenkov counter in the setup equipment is shown in Fig.14.

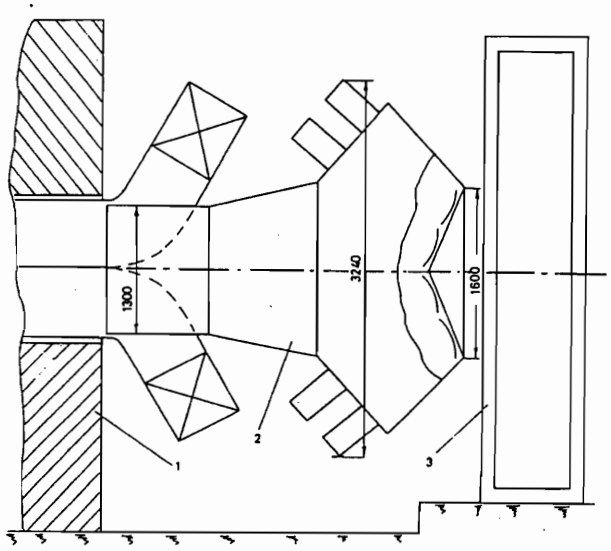

Fig. 14. Scheme of the Čerenkov counter location in the SVD set-up (side – view): 1 – magnet MC-7A; 2 – Čerenkov counter; 3 – movable platform of the detector of γ–quanta.

3.5. The scintillation hodoscope

The scintillation hodoscope (SH) is fastened on a mobile support of the γ-detector at the distance of 8.3 m from the target and consists of two planes of scintillation counters (H_L) and (H_V,) directed horizontally and vertically. The horizontal plane consists of 12 counters having scintillator bands, manufactured by the extrusion method with light-guides on the ends. The dimensions of the sensitive area of a counter are 200×2400 mm and 10 mm thick. The vertical plane consists of 12 counters with the counter sensitive area dimensions of 200×1400 mm. Constructively, the counters are completely autonomous and light–isolated; each counter is equipped with the photomultipliers FEU-110 with a divider valid for high current and has a monitor system of a driver and a lightguide. The hodoscope is assembled on a frame, fastened on the movable support of the γ-detector. If either an access to the γ-detector is necessary, or its calibration in electron beam takes place, the hodoscope can be shifted away in the vertical direction.

The electronics for the readout of signals from the scintillation hodoscope contains 36 signal shapers, 36 strobed registers and selection logics, which includes 5 multientry schemes of coincidence. The slow control system of SH contains 36 channels of slow ADCs. This detector is under construction as part of the first stage of the SVD setup.

3.6. The detector of $\gamma-$quanta

To register π^0-mesons and γ-quanta from charm decay the hodoscopic detector of γ-quanta (DEGA) with radiators from lead glass, which is placed at $\sim$ 8.9 m distance from the active target, will be used. DEGA consists of 1536 Čerenkov full–absorbtion counters with the transverse glass dimensions of 38×38 mm^2 and the length of 505 mm, equipped with photomultipliers FEU-84-3. The total sensitive area of the detector is $\sim (1.8 \times 1.2)$ m^2. A principle of operation of the SVD γ-detector does not differ from that of the detectors with lead glass radiators, used in other IHEP experiments. DEGA is manufactured as an autonomous detector and is established 3 m appart behind the magnet MC-7 on the support, providing a remote–control movement in two transverse–to–beam coordinates. The detector design is based on that of GAMS-4000 [47]. In the data acquisition system of DEGA the computer IBM PC AT 286 and 48 channel ADC Le Croy 2282A are used. They are put in two CAMAC crates, each having the system processor Le Croy 2282 for a preliminary analysis of data. The data acquisition system of DEGA allows one to receive and transmit to the central computer up to 300 words $\times$ s^{-1}.

DEGA provides a registration of γ-quanta in the range of momenta from 300 MeV/c to 20 GeV/c with the coordinate accuracy of 2-3 mm. The spectrometer has the geometrical efficiency of registrating single π^0-mesons from the Λ_c^+ and D decays, which are emitted into the forward hemisphere, in the investigated reactions from 20% to 30%.

The detector calibration is fulfilled in the electron beam of channel 22, having the range of momenta from 5 to 40 GeV/c. Fig.15 shows the distribution of electron energry, obtained during the preliminary calibration of the detector in the electron beam with the energy of 20 GeV/c.

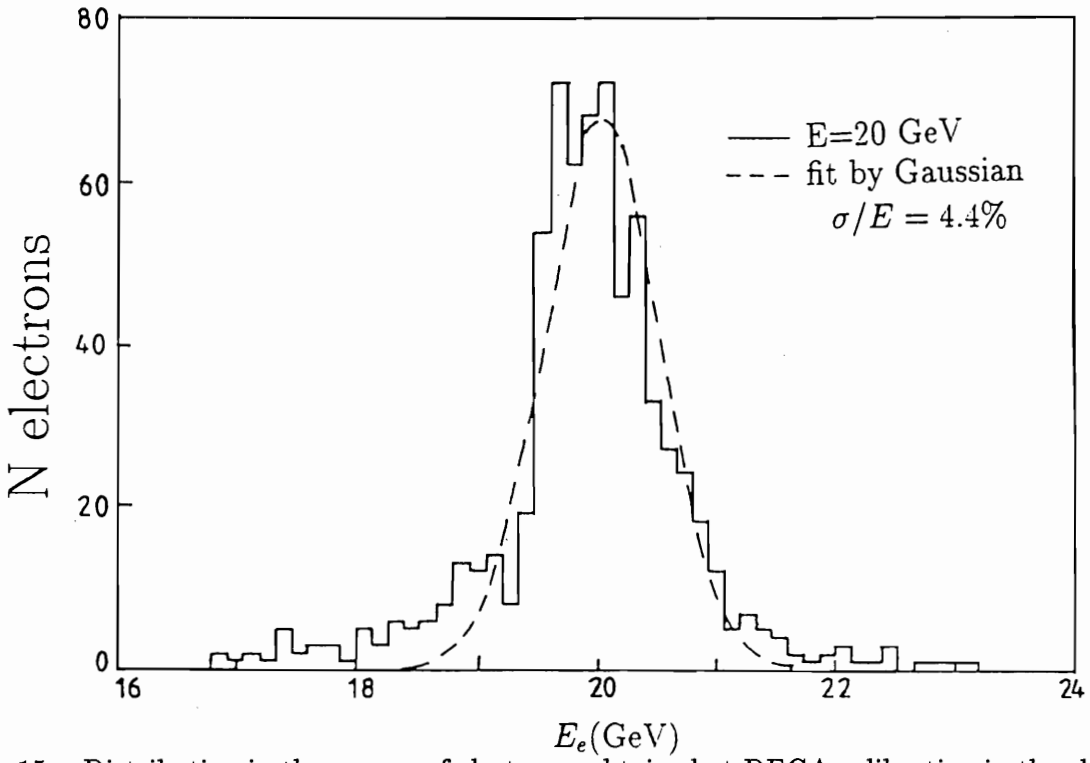

Fig. 15. Distribution in the energy of electrons, obtained at DEGA calibration in the electron beam with the energy of 20 GeV/c.

3.7. The trigger system

3.7.1. Trigger system strategy at the second stage of the experiment

A principal difficulty of the experiment E–161 is a small ($\sim$ 1 μb) cross section of the $\bar{c}c$-pair production due to hard subprocesses in pN-interactions at 70 GeV/c, which comforms to the probability of 10^{-4} of an event with charms appearance in an inelastic pSi-interaction. As it is shown in Section 2.1, a contribution of $\bar{c}c$-pairs due to the mechanism of intrinsic charm release presumably does not exceed this value. Therefore, for accumulation of a sufficient sample of charms an effective selection of the events, containing $\bar{c}c$-pairs, in a real time of the experiment is required.

A similar, but even more complicated problem, has been already encounted in organizing the fixed target experiments to study "beautiful", i.e. b-quark–containing, hadron production in hadron–nuclear interactions, and examples of its successful solution are already known. The approach, developed in the CERN experiments WA 82 [48] and WA 92 [49], appears to be the most promising one. In these experiments the events, having the evidence of a secondary vertex close to the primary one, were selected in the real time of the experiment on the basis of the impact parameter information from the PVD. Therefore, the following two–level organization of the trigger system at the second stage of the experiment is proposed. An efficiency and ways of implementation of this system were studied by the SVD–Collaboration for a few last years.

The first level trigger L1. The first stage of the experiment E–161 has shown that if MSDs are placed both in front of the target and behind it an effective selection of the interactions in this region is possible according to the beam particle absorption criterion [50]. However, the technical implementation of such an event trigger is not simple, therefore at the second stage of the experiment this will be substituted by the event trigger, based on a fast estimation of the amplitudes of signals from the semiconductor counters of AM. This approach will also allow one to determine Z-coordinate of the interaction. Furthermore, as the calculations made in Ref.[51] showed, if the secondary particles were detected in the horizontal bands of the scintillation hodoscope located behind the magnet MC-7A perpendicularly to the beam direction at some distance both above or below the beam, a fast recognition of the events having particles with an increased p_t can be achieved. This allows one to select the events with $(\bar{c}c)$-pairs, the particles from which decays possess of an increased p_t, already at the first level of triggering.

Hence, the trigger $L1$ for AM containing besides the semiconductor counters a sheet of metal foil, is proposed to be organized according to the following algorithm:

A) a value of the signal from the first (protective) counter has to satisfy the requirement $A_0 < 3A_{mip}$;

and

B) a value of the signal from one of subsequent semiconductor counter has to be $A_i > A_{int}$, where A_{int} is the minimal value of the signal due to a pA-interaction, or

C) a value of the signal in the first counter behind the sheet of foil $A_{int} > A_1 > 3A_{mip}$, while $A_i < A_{int}$ in the other counters.

The requirement $A \times B$ defines an interaction in the i-semiconductor counter; the requirement $A \times C$ selects an interaction in the foil.

For a selection of an event, containing a charged particle with an increased $p_t(\geq$ 0.3 GeV/c) the presence of a count in any of the 5 upper (H_L^{1-5}) plates of hodoscope or 5 lower ones (H_L^{8-12}) is needed.

Thus, in the general form the $L1$ algorithm can be written down as follows:

$$C_1 \times C_2 \times \bar{C}_3 \times A \times (B + C) \times (H_L^{1-5} + H_L^{8-12}),$$

where C_1 and C_2 are scintillation counters for the detection of a beam particle and C_3 is a scintillation veto counter with a slit, which are placed in front of the PVD.

The Monte–Carlo simulation showed that the efficiency of this trigger for the events with charms is 0.5, while for the background events it is 0.16, i.e. the 3–fold enrichment of the sample by charmed events can be achieved.

The decision time on L_1 trigger, τ_1, must not exceed 200 ns.

The second level trigger L2. The trigger $L2$ is based on a fast estimation of the secondary charged particle trajectory impact parameter relative to the primary vertex. The algorithm is supposed to be realized as a sequence of the following operations (steps). Only the estimation of the impact parameter in the axis Y is described as an example; the impact parameter in the axis X is determined in the analogous way:

I. Readout of the initial data to the computer memory from the lower level equipment.

II. Determination of the Y_v-coordinate of the interaction in an active target.

In the computer memory two–dimensional arrays for each detector $D(i)$ of the active target are created. Their elements are the precalculated values of the Y-coordinate in the given AT detector depending on the channel numbers of two forward beam detectors (MSD_1 and MSD_5).

Thus, choosing the described above array in accordance with the received number of the active target detector (in which an interaction was observed) and tracking out the element from this array with the indices corresponding to the numbers of the strips giving counts in two forward MSD planes, we directly determine the Y_v-coordinate of an interaction.

III. Calculation of the impact parameter for the track candidate.

In order to fulfill this procedure for each detector of AT the arrays, similar to ones, described for step II, are created in the computer memory. However, these arrays are calculated for the planes MSD_7 and MSD_{11}, placed behind the target.

Thus, choosing the channels with counts in these planes and the array in the number of the detector $D(i)$, we directly obtain the Y-coordinate of the track candidate intersection with the vertical plane, containing an interaction. As a result the following three options arise:

1. Difference between the Y_v-coordinate and the calculated coordinate exceeds the upper limit, imposed on an impact parameter size. In this case the track candidate is eliminated, the next pair of counts depending on the direction of the eliminated track is selected, and step III is repeated till all counts are exhausted.

2. Y-coordinate coincides (within the given error bar) with the interaction coordinate. In this case we have the candidate for a secondary track produced in the primary vertex, which is also eliminated from the further consideration. Then step III is repeated for the next pair of points.

3. Y-coordinate difference fits the range, allowed for the impact parameter. In this case we may assume that the investigated track candidate is the one produced in a secondary vertex and pass on to the next step.

4. Verification, if the track candidate is a real one. For each pair of points of MSD_7 and MSD_{11} planes a two dimension array is created whose elements are the coordinates of an intersection of the straight lines, drawn through all possible combination of Y-counts of the given pair of MSDs, with the plane of MSD_9.

After selecting from the given array the element with the indices, conforming to the pair of points chosen at step III, we verify if there is the count in the middle plane lying close to the point of intersection of the straight line, drawn through this pair. If so, we deal with a real track and turn to the next step. If not, the next pair is chosen and step III is repeated.

5. Reaction to the control electronics. Depending on an outcome of the algorithm execution (i.e.,whether a track with the given impact parameter is found or not) an appropriate signal is transmitted to the control equipment.

Step 4 is not compulsory for the passing of the algorithm. As the results of the Monte Carlo simulation showed [52] the selection of the events with charm particles on the basis of one track with a large value of the impact parameter is not very effective at the energy of the proposed experiment and making use of information of all particles detected in the PVD is preferable. The final choice of the $L2$ trigger organization can be made, only after experimental investigations with the really working equipment. The time characteristics of this algorithm are given in Table 3.

Table 3
Decision time of the algorithm and required sizes of the fast memory (for the 32-bit processor with 100 MH clock).

Steps	Time, μs	Memory, Mb	
		10 detectors	20 detectors
I	70	-	-
II	15	0.64	1.28
III	100	5.12	10.24
IV	100	1.024	1.024
V	15	-	-
All	300	~ 7.0	~ 13.0

The time of the algorithm performance by a processor with other clock frequency changes proportionally to it.

An efficiency of the algorithm performance can be significantly improved, if it is applied in two orthogonal projections simultaneously. In this case a decision time increases by a factor of 2. An application of two simultaneously working processors is also possible for this scheme without changing the decision time.

In Fig.16 the distributions of the maximal impact parameter Δ_{max} (in any axis) are shown for events with charms (the dashed histogram) and for background events (the solid histogram) simulated for AM, consisting of the W foil 250 μm thick and of 4 Si counters 330 μm thick each, for the PVD construction, described in Part 3.1. To make a comparison convenient the areas of both the distributions are normalized to 1, which corresponds to the multiplication of the distribution for events with charmed particles by a factor of 6.6×10^3. It is seen, that the distribution in Δ_{max} for the background events rapidly falls to about 200 μm and further has a "tail" of single events with large impact parameters, which is caused by secondary interactions and strange particle decays. Cutting $\Delta_{max} > 100$ μm provides about 10–fold enrichment of the sample by the events with $\bar{c}c$-pairs (without taking into account the enrichment provided by $L1$), with about 55% of the total number of such events retained in the triggered sample.

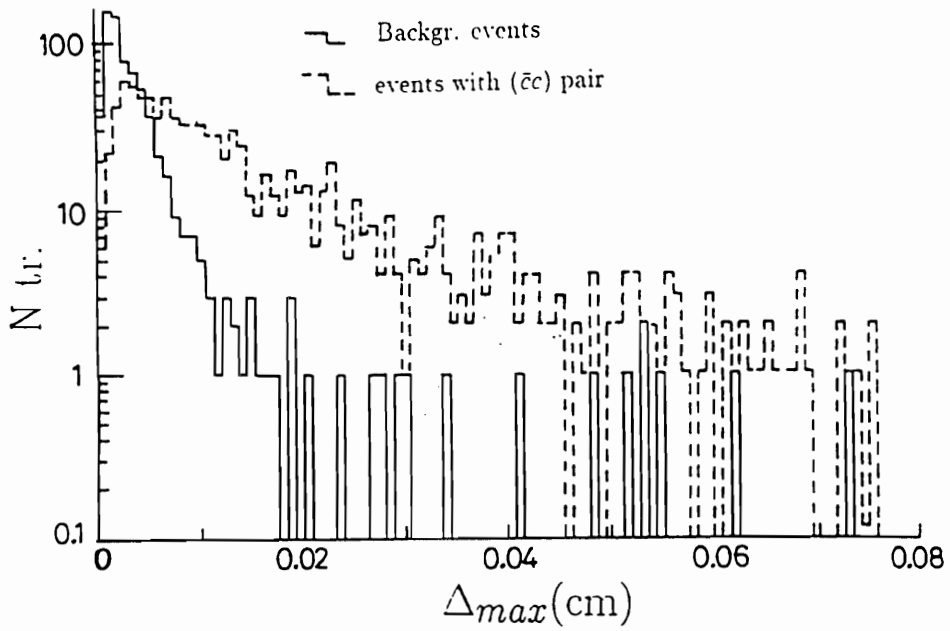

Fig. 16. Distributions of Δ_{max} for the events with charms (the dashed histogram) and background events (the solid histogram), normalized to the unit area.

Additional investigations showed that a significant width of the distribution Δ_{max} for background events was caused by the bending of a trajectory of the low momentum charged particles because of multiple scattering in AM and T_2. Under simulation (and in a real trigger) a part of such slow particles can be eliminated by additional selection of the straight tracks in the planes $YZ(XZ)$ passing via T_2 counts. It is based on the requirement, that a real count in $MSD_{9(10)}$ should deviate by no more than one pitch value from that, predicted for a straight line drawn through corresponding counts in $MSD_{7(8)}$ and $MSD_{11(12)}$. However the problem of suppression of low momentum charged particles, suffering a significant multiple scattering, requires further study, which can lead in future to some changes in the PVD construction, described in Sect. 3.1.

As it was shown in Ref.[52], an improvement of a signal (i.e. of events with charmed particles) extraction in the presence of a background is possible also due to the $L2$ algorithm optimization by using the impact parameter information for all particles, reconstructed in T_2. The sum Σ of all impact parameters, weighted in a certain way, must be used as a variable, according to which the selection is made.

In Fig.17 a probability of the events with $\bar{c}c$-pairs to pass through trigger $L2$ and of sample enrichment by such events is shown as a function of Σ. It is seen that with the proposed trigger system the $\Sigma > 1.3$ cut ensures more than 50–fold enrichment of the sample with retaining in it 30% of the initial amount of the events with $\bar{c}c$-pairs.

The detailed investigations carried out in Ref.[52] showed, that the $L2$ algorithm most effectively reacts on three–particle decays of $D^{\pm}$-mesons and on four–particle decays of D^0-mesons. But only about 12% of decays of shortliving Λ_c^+-baryon can be selected by $L2$ trigger.

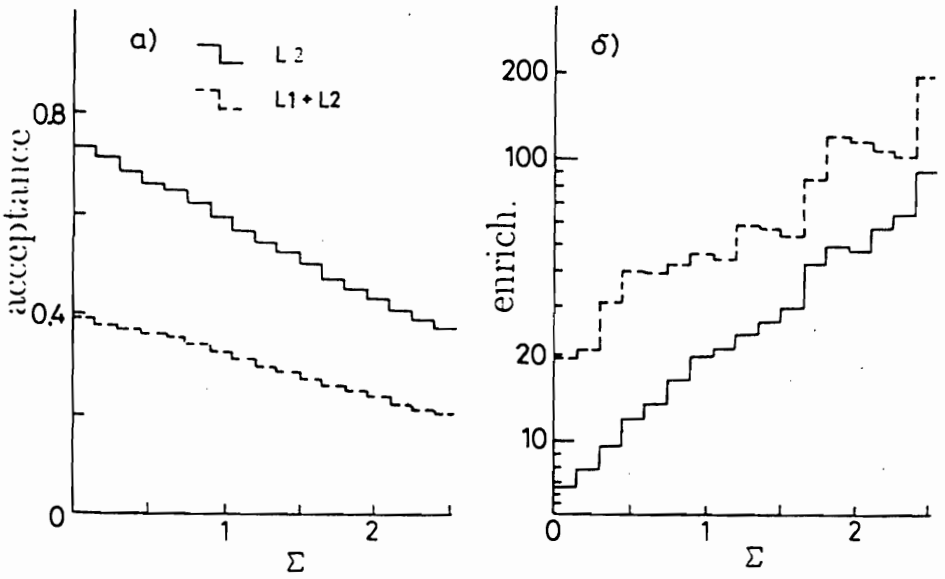

Fig. 17. Dependence on Σ parameter a)of the probability of passing of such events through the trigger $L1 + L2$ and b)of the enrichment of the sample by the events with charms.

Fig.18a shows the ratios of various charm x_F-distributions from the events, which have passed $L1+L2$, to the distributions of these particles in the initial sample of the simulated events. In Fig.18b the analogous ratios of p_t-distributions are given. It is seen that the proposed trigger system does not lead to a significant dependence of the events selection probability on the variables x_F and p_t.

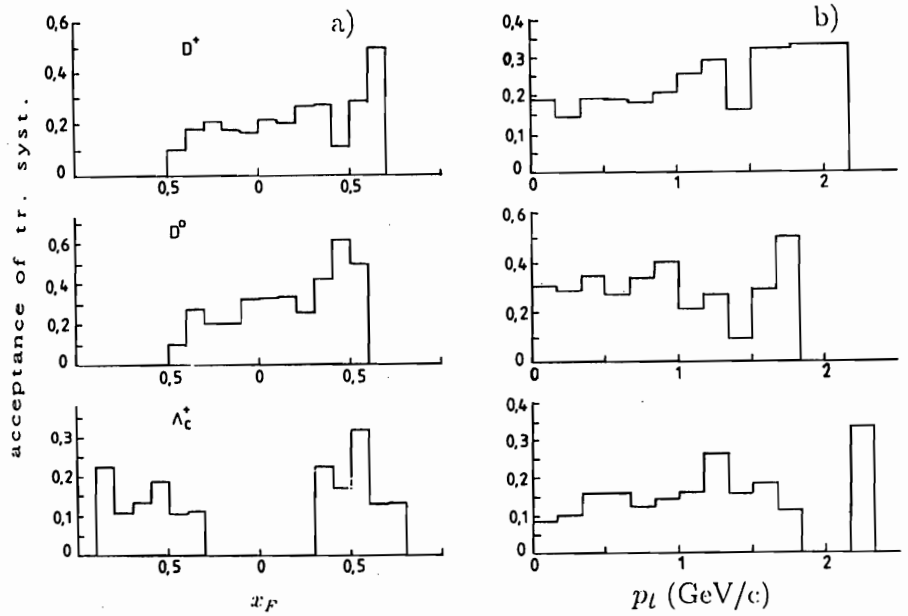

Fig. 18. a) Ratios of x_F-distributions of D^+, D^0-mesons and Λ_c^+- baryons, having passed $L1 + L2$ to the distributions of these particles in the initial sample; b) Similar ratios for p_t-distributions.

3.7.2. Electronics of the trigger system

Taking into account a short decision time of $L1$ and in order to reduce a total length of signal cables it is proposed to place the beam monitoring electronics as well as the data acquisition and processing electronics for $L1$ and $L2$ triggers in the immediate proximity to the PVD, where the electronics will be within the reach during a run without closing the beam stopper. The electronics of the encoded data transmission for the $L2$ trigger is supposed to be housed in an experimental hut.

Beam monitoring electronics. A primary monitoring of the beam is supposed to be fulfilled using the scintillation counters, placed in front of the PVD. The signals from the scintillation counters after shaping and processing by the fast logics are transmitted to the beam monitoring system scalers for subsequent processing and presentation of data in a separate computer PC IBM-486, linked with the central computer through the ETHERNET network. The starting signal worked out by the beam monitoring system and referred later on as "monitor" can be transmitted to each subsystem of the set-up for its autonomous testing.

L1 electronics. Signals from the active target semiconductor counters after preamplifiers are transmitted to the 4–channel module COMP, containing discriminators with program–controlled thresholds. An interaction in any of AT detectors results in a signal exceeding the threshold in COMP. The information from it then follows to $TP1$ module for $L1.1$ signal formation. The fired AT detector number is transmitted for the subsequent processing by the $L2$ trigger electronics.

The signals from the scintillation hodoscopes after amplifiers–discriminators are also transmitted to the $TP1$ module, where after the coincidence with the beam control scintillation counter signals, they take part in the $L1.2$ signal formation. The total decision time for $L1$ is within the 200 ns limits with respect to the instant of a beam particle passing.

L2 electronics. The $L2$ electronics is intended for the primary processing of the signals from the planes of $MSD_{1,2}$, $MSD_{5,6}$ and MSD_{7-12}, encoding the data and transmitting significant data to fast memory of one or more computers for subsequent processing according to the algorithm, described in section 3.7.1.2. In the case of the positive decision on $L2$, the information of the hitted strips of these planes is transmitted through the ETHERNET network to the main computer of the set-up. The functional scheme of the $L2$ electronics modules is given in Fig.19.

For the data read out from the planes of $MSD_{1,2,5,6}$ as well as from the planes MSD_{7-12} it is supposed to use AMPLEX chips with 16 channels per chip. Each channel of AMPLEX has a low–noise charge amplifier which is followed by a shaper. The time of the shaper sample–and–hold can be regulated in the range of 150–300 ns and can be used for a signal

delay. When the appropriately timed strobe signal comes to sample–and–hold stage the analog values are stored for each entry. In order to read out 16 analog values the multiplexer $16 \rightarrow 1$ and an exit buffer are used. The readout can be performed at the rate of 6 MHz. The time of the AMPLEX reset is 2 μs.

The basis of the system, preparing data for $L2$ trigger, is provided by Amplitude Analysing (AA) modules. The functional scheme of an AA-module is shown in Fig.20. The 8 – channel module processes the signals from 128 strips of silicon detectors and includes the following components:

1. 8–bit ADC
2. Data Fast Memory (FM)
3. Standard FM
4. Hit FM
5. 8–bit digital comparator
6. Address Counter (AC)
7. Multiplexer (M)
8. Bus Driver (BD)
9. Steering scheme.

The analog signal from a MSD strip, having been processed in AMPLEX, is transmitted by a co–axial cable to an AA module. The information about the signal amplitude is written down in the data FM, having a depth of 16 the 8–bit words, according to pulses of a clock generator of the AMPLEX readout. Then it is used for a further off-line analysis. Simultaneously the data from an ADC output are compared in the comparator to the standard value of this channel amplitude, stored in the standard FM, having the same capacity. The information about the number of a hitted strip is written down in the Hit FM having the depth of 16 the 4 – bit words. The address of this FM is determined by the Address Counter. The reading of the Hit FM proceeds subsequently through a Multiplexer and a Bus Driver, provided one of eight Address Counters has brought forward a request at BUS 1.

A procedure of analog signal processing in AMPLEX, digitilization in ADC and storing in Hit FM takes 3 μs. The encoding process takes place simultaneously in all AA modules. Thus, in about 3 μs after an interaction the information about hitted strips is ready for reading through BUS 1, Interface Card 1 (IC1), BUS 2 and Interface Card 2 (IC2) in a trigger computer. The COMP module, storing the information about the position of the detector of AT, provided a signal, is also available for reading through BUS 1. The interrelation of the $L2$ electronics with other parts of the set-up is organized with use of TP_2 module, reachable by BUS 1. It is supposed to place the AA modules and IC1 as close as possible to the detectors, and IC2 – in the computer, taking decision on $L2$. It is supposed to provide a rate of 16–bit data transmission through BUS 2 not less than 0.5 MHz. In this case the rate of the data transmission will be 1 Mbyte/s, and a total time of the data transmission for the event multiplicity equal 10 will not exceed $60 - 70$ μs.

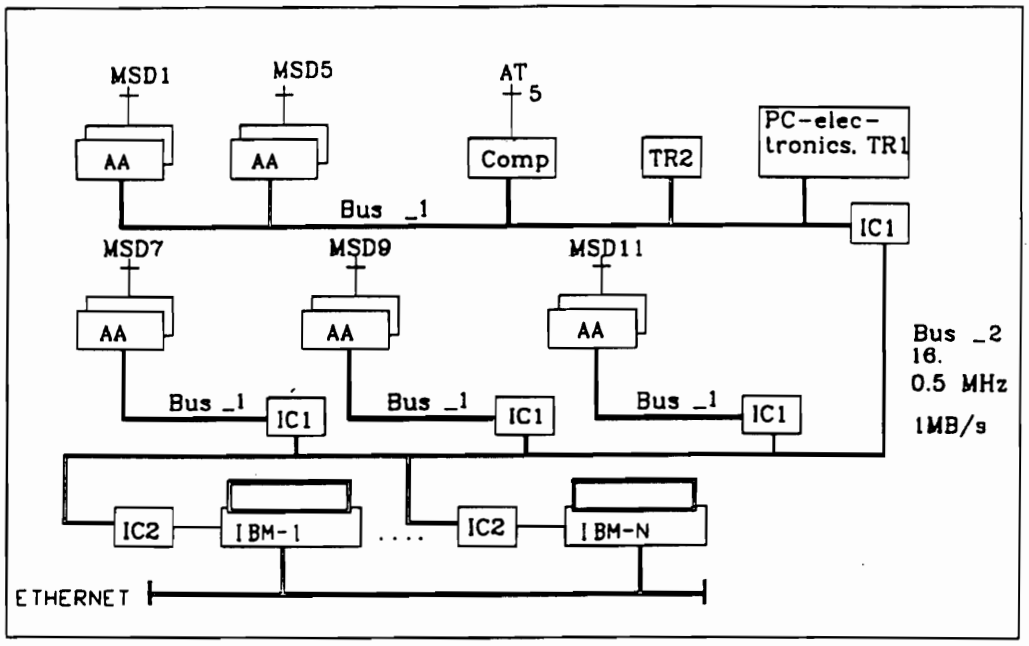

Fig. 19. Functional scheme of the $L2$ subsystem modules for a Y-coordinate.

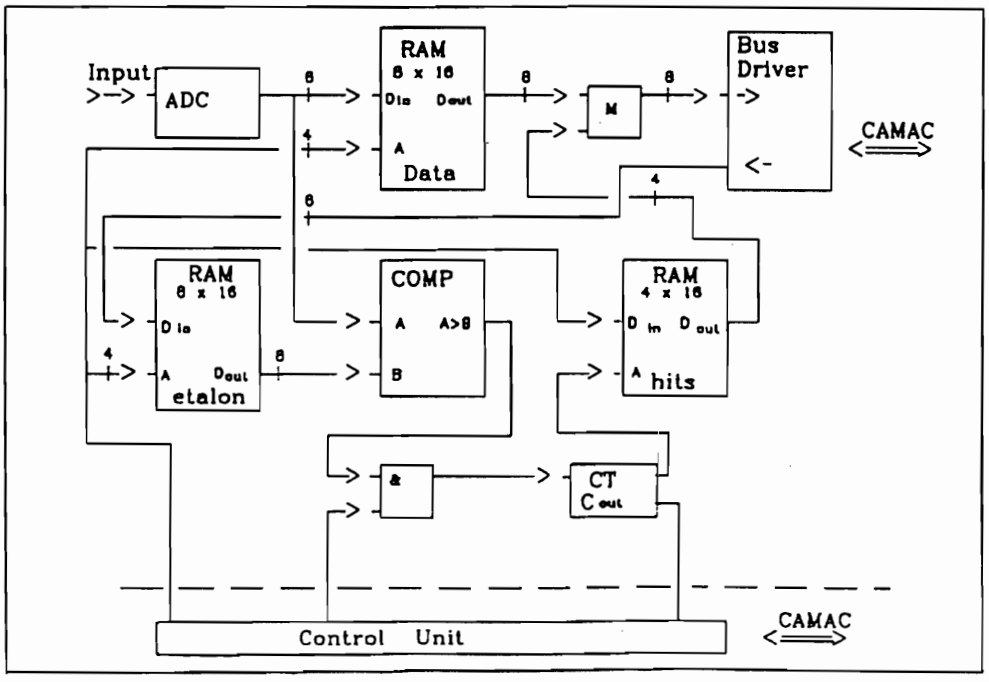

Fig. 20. Functional scheme of an AA module for AMPLEX readout.

3.8. Data acquisition system

3.8.1. Main trends of data acquisition hardware upgrade

The hardware and the software of the system of the data read out from the SVD detectors is planned to be modified in the following way:

– significant increase (at the minimum, by an order) of the reliability of the used computer hardware;

– significant increase of the size of fast and disc memory of on-line computers, allowing one to enlarge the amount of the readout data for an accelerator spill;

– introduction of local communication networks between on-line computers of various systems of the set-up, which would eliminate restrictions in the data acquisition system and in the control for the apparatus performance;

– introduction of two modes of operations of the magnetic spectrometer:

a) a working mode, ensuring of acquisition of 200-300 words per event at a rate up to 400 events per spill;

b) a testing mode, ensuring an acquisition of histograms with a peak rate no lower than 100 KB/s;

– increase of numbers of readout channels due to the introduction of new triggering subsystems;

– improvement of the quality of service and diagnostic programs, testing equipment as well as slow control systems;

– providing the modern level of the results presentation during the runs (colour and multi – dimensional graphics).

The front–end and DAQ hardware at the 2nd stage of the experiment E–161 will consist of the following systems:

1) beam monitoring system;

2) data holding from the new trigger subsystems of the 1st and 2nd level;

3) electronics of the magnetic spectrometer with MWPCs (mainly taken from the 1st stage of the experiment);

4) electronics of the Čerenkov threshold counter;

5) electronics of the multichannel Čerenkov detector of $\gamma-$quanta (taken from the 1st stage of the experiment);

6) system providing of the test signals and slow control of subsystems parameters;

7) central system of data storing and visualization.

An expected intensity of data flows (after the 2nd level trigger) for the main SVD detectors is:

1) precision vertex detector – 15 KB/s;

2) magnetic spectrometer – 30 KB/s.

Five personal computers IBM PC/486 with a clock frequency not less than 30 MHz, a fast memory not less than 8 MByte and a 300 MByte disc must be included in the subsystems 1)-5) as DAQ and control computers.

A working station ALFA (DEC) or INDY (Silicon Graphics) with the parameters: the clock frequency 100-150 MHz, a fast memory 64 MByte, a disc memory no smaller than

2 GByte, a colour monitor of 17 inches screen are to be a basis of the subsystem for collection and organization of data from various detectors.

The data acquisition subsystem must be based on the local network ETHERNET with the rate of data transmission 10 Mbyte/s.

3.8.2. On-line software organization

When upgrading the apparatus it is supposed to completely renew the computers, used for on – line processing of data, to change the network hardware, to include new devices and detectors, such as the precision vertex detector, the multichannel Čerenkov counter, the slow control system, etc.

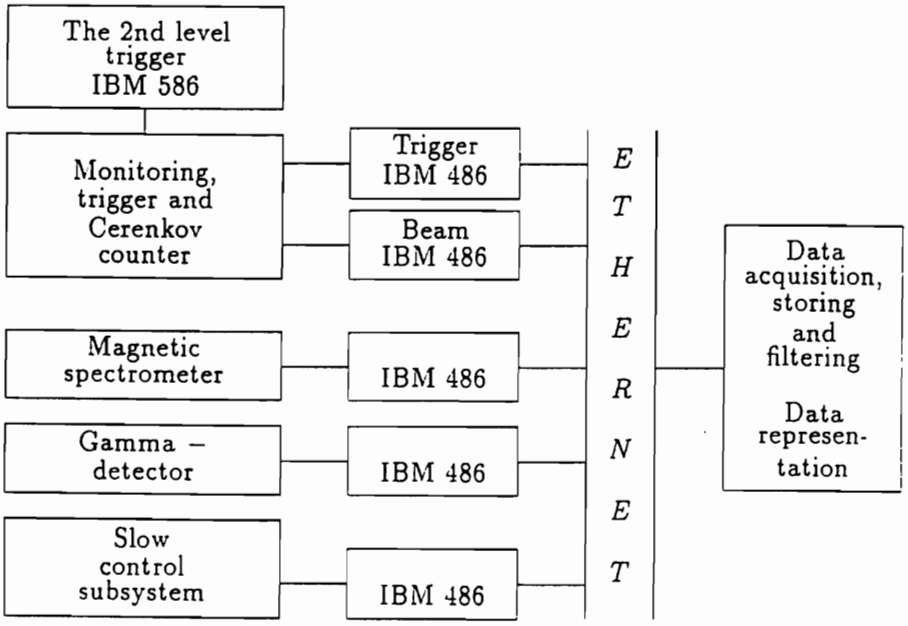

Fig. 21. Scheme of the organization of computers and information flows for the second stage of the experiment E-161.

In order to provide the readout of information and the upgraded set-up control the scheme of the computer hardware organization and information flows, outlined in Fig.21, is proposed. For the realization of this scheme it is necessary to develop the software which provides:

1) testing of electronic units and modules (amplifiers, interfaces, controllers, etc);

2) testing of separate parts and subsystems of the setup (the $L1$ and $L2$ trigger equipment, spectrometer, unified synchronization scheme, etc);

3) the means for testing works before and during the physical runs with the data collection (a work with a radiation source, a delayed coincidence curve registration, a calibration, etc);

4) beam monitoring programs;

5) programs of the control of the $L1$ and $L2$ subsystems;

6) programs for operating the subsystem of the slow control of the set-up parameters (power supplies, gas mixture control, etc);

7) programs of the data collection and assembly during a physics run;

8) event selection programs (filtering at the upper level computer).

All the new programs described above are supposed to be complemented by modern means of data presentation (histograms, graphs, event screens) and by the highest capacity interactive user interface, realized by X Window with OSF/MOTIF package application.

4. OFF-LINE DATA PROCESSING

4.1. The principles of the charm decays reconstruction

A large number of charm decay channels, among which a significant share of multiparticle decays with neutral hadrons takes place, makes difficult a complete identification of each charm decay. This leads to the situation, when at mass processing of data in the experiments on charm hadroproduction at high energies only the neutral charm hadron two–article decays and charged charm hadron three–particle ones are usually reconstructed [16,17,29].

However, as the experience of data processing in the experiment NA27 at the EHS [15] showed, having the information on the secondary vertex coordinates and the possibility to connect directly the charged particle tracks with this vertex, a large sample of multiparticle hadron decays can be efficiently reconstructed with the use of the known procedures of the kinematic fit of different hypothesis. The data processing in the proposed experiment is supposed to be organized by using this principle. Therefore, it must include the following stages:

A. Stricter selection of the events with possible nearby secondary vertices by a filtering program which checks satisfing the trigger requirements on the basis of a more accurate reconstruction of the straight tracks in PVD by using information from all its detectors.

B. Reconstruction of coordinates of any secondary vertex and connection with it of the secondary charged particle tracks, using the data from the PVD.

C. Geometrical reconstruction of tracks, based on the coordinate information from MSDs of the PVD trigger part, as well as on the data of the magnetic spectrometer track system, and determination of their momenta.

D. Measurement of the energy and the angles of $\gamma-$quanta in DEGA.

E. Reconstruction of the invariant mass of particle system from secondary vertex and selection of the most probable hypothesis for charm hadron decay by the kinematic fit.

F. Search of the second charm hadron in combinations of the rest of secondary charged particles and $\gamma-$quanta.

A basis of this processing system will be both avialable and adapted for the SVD set-up programs of the geometrical reconstruction of tracks in the magnetic spectrometer (TRIDENT version 504) as well as the program for kinematic fit (HYDRAKINE).

At this stage of the experiment the programs, developed for the experiment WA92 and granted us by this Collaboration, will be used for both the geometrical reconstruction of

straight tracks in the PVD and their linking with parts of the tracks, restored in the magnetic spectrometer.

In order to search for the second decay vertex the method of the interactive processing of data, also developed in WA92 Collaboration, will be accepted. Using the program of the graphical analysis of events with elements of estimates of some kinematic parameter the counts from both MSDs of the PVD and MWPCs of the spectrometer can be displayed along with the images of the reconstructed tracks for their visual checking. Furthermore, using additional guide points, it will be possible to change the results of the track program reconstruction and of the track linkage to introduce new vertices to verify a possibility of the track connection to various vertices, to estimate transverse momenta balance at the given vertex etc.

4.2. Possibilities of the event topology reconstruction by using the PVD data

For a more strict selection of the events with possible secondary vertices, using the data from MSDs and CCD of PVD, the Z_v-coordinate of the primary vertex must be determined more accurately with the use of the spacially reconstructed straight tracks, and a selection of the tracks, which do not emerge from the primary vertex, must be made. To estimate an accuracy of Z_v-coordinate determination, using the PVD data for the simulated background events, straight lines were drawn through $X-$ and Y-counts in $MSD_{1-12,14,16}$ and CCD by the least square method (LSM), and the primary vertex coordinates were determined more accurately as a result of LSM minimization of the sum of square distances of the vertex to primary and secondary tracks. To reduce the influence of the slow particles, having suffered a strong multiple scattering in AM and $T2$, the iterative process of the vertex coordinate determination was used, excluding from the consideration the track with the maximal impact parameter for each of the procedure repetition. In Fig.22 the distribution of the deviations between the measured Z_{meas}-coordinate and veritable one (Z_v), as well as the similar distribution for $X(Y)$-coordinates, are given. It is seen, that the primary vertex Z_v-coordinate can be restored with the accuracy to about 80 μm. For the background events a more accurate determination of the primary vertex Z_0-coordinate and, hence, a reduction of the secondary track impact parameter value relative to it allows for the significant (as a factor of 2-3) reducing of a number of false triggers. Simulation showed, that for the events with charm decays the accuracy of Z_v reconstruction is worse (~ 90 μm), but secondary vertices, distant from the primary one at $L \geq 400$ μm, must be distinguishable from it. In Fig.23 the decay lenght distributions of $D^{\pm}$, $\bar{D}^0$ and Λ_c^+-baryons are given. The distribution the decay lengths of fast (with $x_F > 0.5$) Λ_c^+- baryons, corresponding to such ones which have been produced through the intrinsic charm mechanism, is shown separately. It is seen, that the vertices from neutral and charged D-meson decays will be mainly reconstructed, while the decay vertices of Λ_c^+-baryons will mostf requently merge with the primary vertex.

The vertices from D-meson decays in two or more charged particles theoretically can be also found as a point of intersection of two or more charged particles, non–included in the primary vertex. However, the presence of both the two vertices from charm decays and

the slow particles from the primary vertex, having suffered a strong multiple scattering, makes this procedure ambiguous. Therefore a special algorithm of finding three points of intersection of the charged particle trajectories, restored in PVD, will be worked out.

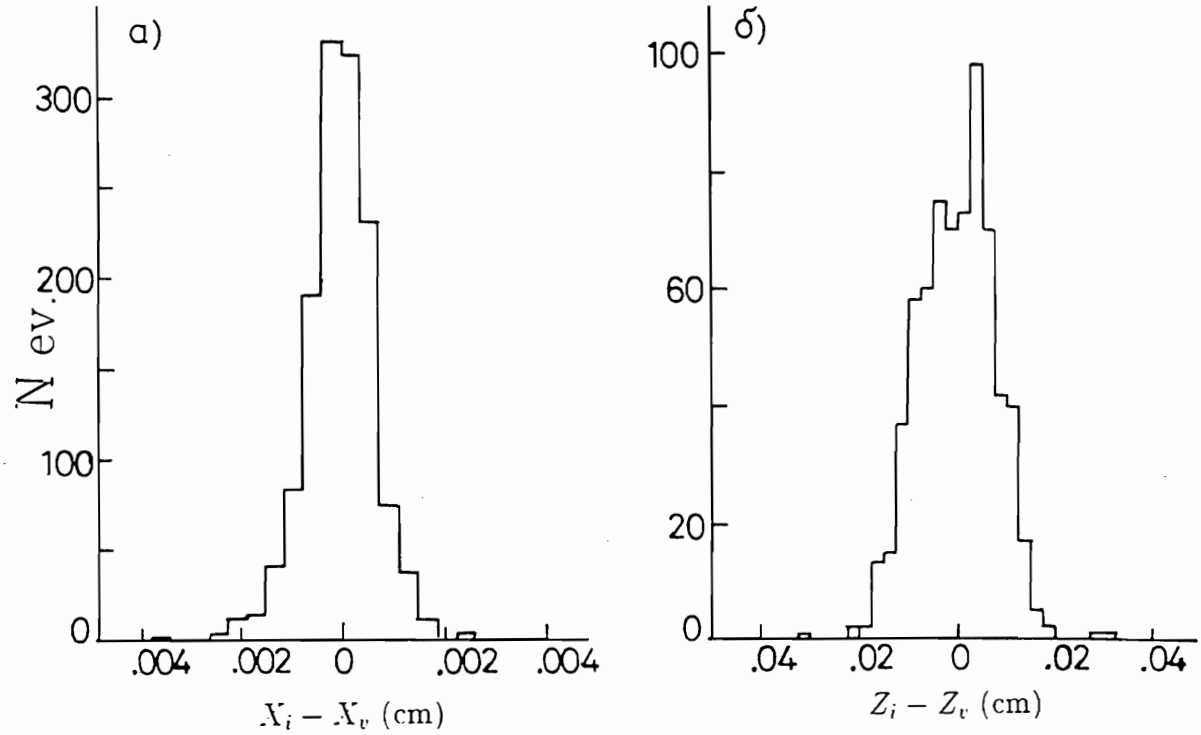

Fig. 22. Distributions of the deviations between the veritable and reconstructed coordinates of the primary vertex in the axes: a)$X(Y)$; b) Z.

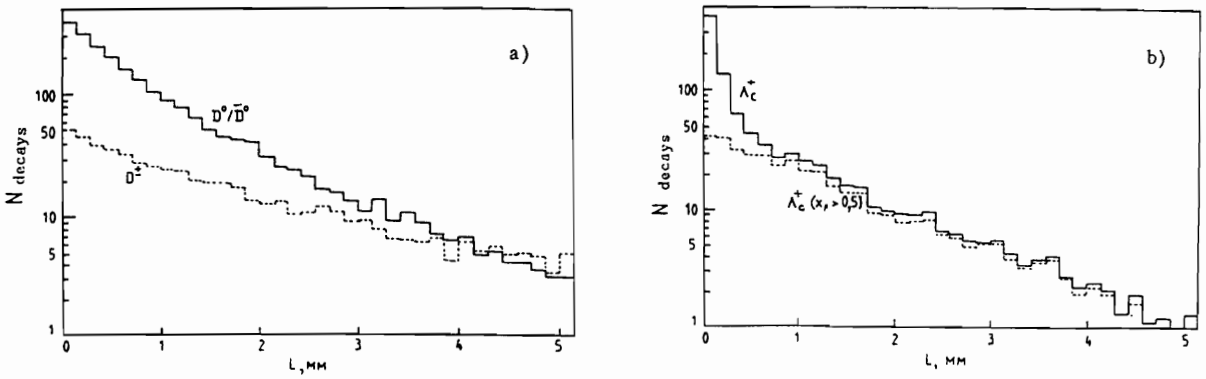

Fig. 23. Distributions of the decay lengths of D^+, D^0-mesons and Λ_c^+- baryons from pA-interactions at 70 GeV/c.

4.3. Efficiencies of the reconstruction of various modes of the charm hadron decay

Because of small decay lengths L of charm hadrons even when a decay vertex is reconstructed generally only a poor estimate of the charm production angles can be obtained. In this case, at the kinematic fit of the decay hypothesis the 3–momentum of a charm hadron must be considered as completely unmeasured, and only one kinematic constrain remains (so called 1C-fit – hypothesis). It may be used as a restriction for a particle mass, providing that the 3-momenta of all the decay particles have been measured accurately enough. Therefore, an efficiency of the charm detection in the apparatus is determined by both a probability of measurement in the magnetic spectrometer of all the charged products of decay and a probability of restoration in DEGA of parameters of the decay π^0-meson.

The estimates of these probabilities were obtained at simulated events with a charm pair, which decay products were propagated through SVD detectors using the program GEANT. As the measured charged particles only such ones were taken, which passed no less than three quadruplets of the track system detectors, and which momenta were measured with an accuracy better 25%. The γ-quanta from a π^0-meson decay in DEGA were considered as the measured ones, if they had hit the array of the radiators of the full absorption Čerenkov counters.

The main hadronic decays modes of D-mesons and Λ_c^+-baryon and the calculated probabilities of their detection by the SVD are given in Table 4.

Table 4

D^+-meson decay modes	Detection probabil.	D^0-meson decay modes	Detection probabil.	Λ_c^+-baryon decay modes	Detection probabil.
$D^+ \to \bar{K}^0\pi^+$	0.09	$D^0 \to K^-\pi^+$	0.37	$\Lambda_c^+ \to pK^-\pi^+$	0.47
$\to K^-\pi^+\pi^+$	0.39	$\to \bar{K}^0\pi^+\pi^-$	0.12	$\to \Lambda\pi^+\pi^+\pi^-$	0.21
$\to \bar{K}^0\pi^+\pi^0$	0.04	$\to K^-\pi^+\pi^0$	0.14	$\to \Lambda\rho^+$	0.13
$\to \bar{K}^0\pi^+\pi^+\pi^-$	0.10	$\to K^-\pi^+\pi^+\pi^-$	0.40	$\to \Sigma^+\pi^+\pi^-$	0.16
$\to K^-\pi^+\pi^+\pi^0$	0.13	$\to K^-\pi^+\pi^+\pi^-\pi^0$	0.12	$\to p\bar{K}^0$	0.14
$\to K^-\pi^+\pi^+\pi^+\pi^-$	0.37	$\to K^-\pi^+\pi^0\pi^0$	0.06	$\to p\bar{K}^0\pi^+\pi^-$	0.13

In Fig.24 x_F-distributions of the simulated D^+-mesons, decaying through the channels $D^+ \to K^-\pi^+\pi^+$, $\to K^-\pi^+\pi^+\pi^0$ and D^0-mesons, decaying through the channels $D^0 \to K^-\pi^+$, $\to K^-\pi^+\pi^0$, are given. The dashed regions in these Figures conform to the decays, all the particles from which have been measured in the SVD spectrometers. It is seen, that in the region $x_F > 0.2$, being of the main interest in the light of the physical tasks described in Sect. 2, the efficiency of the reconstruction of the decays without π^0-emission is sufficiently high.

For the decay lengths $L \geq 1$ mm an accuracy of the angle determination of a primary charm hadron must be better than 10 mrad, which allows for kinematical reconstruction of the charm decays, measured non completely. This should increase the detection efficiencies given in Table 4.

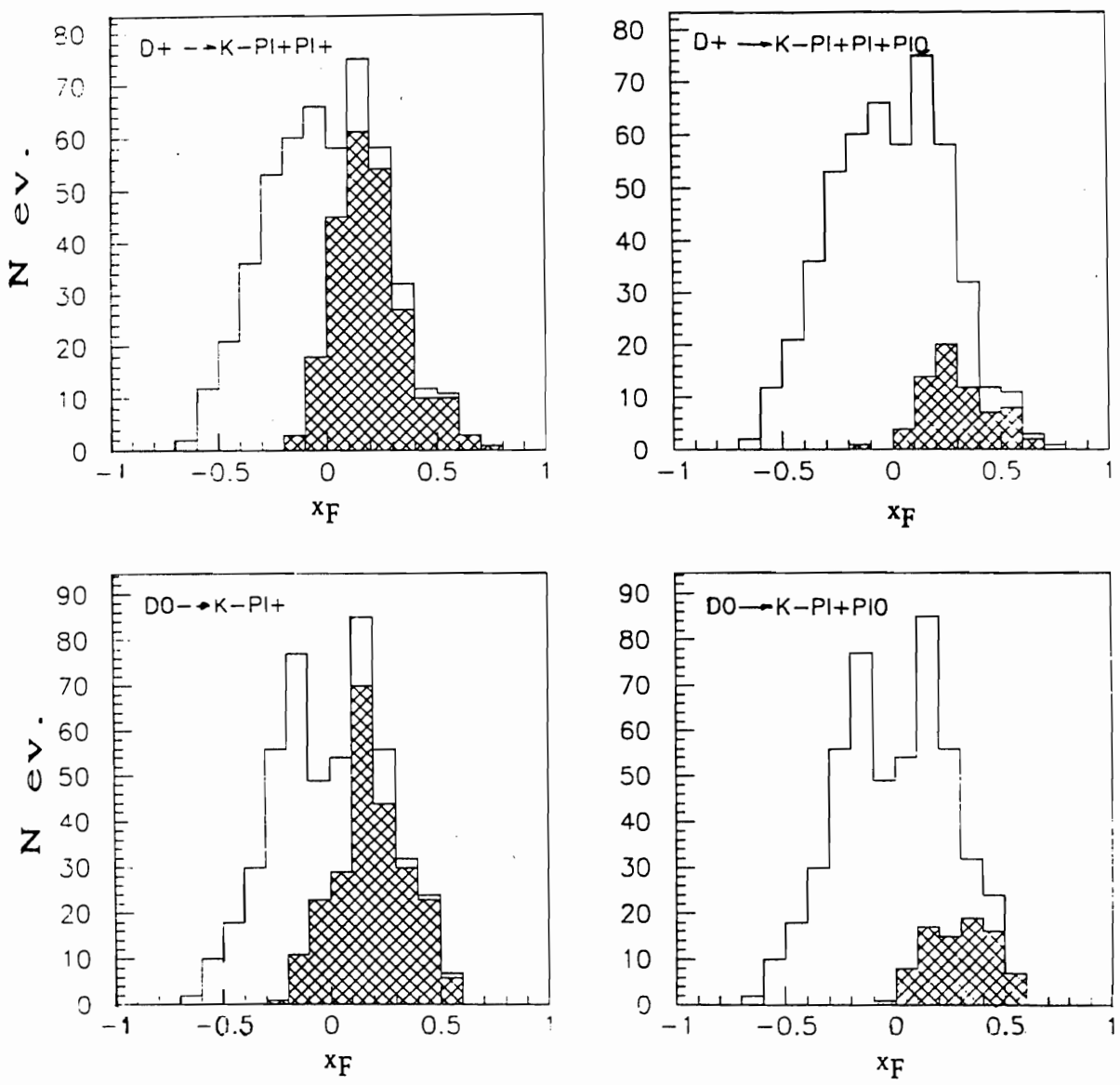

Fig. 24. Distribution in x_F of D^+-mesons, decaying through the channels $D^+ \to K^-\pi^+\pi^+$, $\to K^-p\pi^+\pi^+\pi^0$, as well as of D^0-mesons, decaying through the channels $D^0 \to K^-\pi^+$, $\to K^-\pi^+\pi^0$, and x_F-distributions for these decays, completely reconstructed in the apparatus.

5. EXPECTED RATES OF STATISTICS ACCUMULATION

Accurate experimental data on the cross section of charm hadroproduction in the nearthreshold region so far have not been obtained yet, nevertheless the existing experimental estimates do not contradict to the results of the QCD calculations, which predict $\sigma_h(\bar{c}c) \sim 1\ \mu b$ in pN-interactions at 70 GeV/c.

Therefore, at prognostication of the charm production in pA-interactions at the 2nd stage of the experiment E–161, the value $\sigma_h(\bar{c}c) = 1\ \mu b$ was taken for the QCD cross section of $\bar{c}c$-pairs production in the hard subprocesses and the results of the calculations, made in Ref.[18], were taken as an estimation of $\sigma_{intr}(\bar{c}c)$. As it is shown in Sect.3, in order to provide an effective selection of the events with $\bar{c}c$-pair in the real time of the experiment, AT must be rather thin for reducing the multiple scattering of the secondary hadrons. With the AT pattern, considered in the Proposal (the W foil with the thickness 0.0026λ and 4 counters of Si with the same total thickness), and at the proposed above cross sections of $\bar{c}c$-pair production in a proton beam with the intensity of 3×10^6 p/s having the diameter of the beam cross–image of 3 mm on AT about 1.5×10^4 int/s takes place in AT, among them being at least three events with $(\bar{c}c)$-pair.

At a beam spill in a second at the proton synchrotron U70, the statistics given in Table 5, can be obtained for 24 hours of an uninterrupted operation.

Table 5

	Total number of the events		Number of the events with $(\bar{c}c)$	
	for spill	for 24 hours	for spill	for 24 hours
From the target	$1.5 \cdot 10^4$	$1.4 \cdot 10^8$	3	$2.9 \cdot 10^4$
After L1	$2.5 \cdot 10^3$	$2.4 \cdot 10^7$	1.5	$1.4 \cdot 10^4$
After L2	90	$8.6 \cdot 10^5$	0.9	$8.6 \cdot 10^3$

In order to estimate the statistics for each particular decay of charms from the reaction (1)-(4), their relative yields predicted for hard QCD–subprocesses by PYTHIA program, can be used. In the table below the percentage of the events, containing a charm hadron of the given type (with the exception of $\overset{(-)}{D}_s$-mesons) is presented.

Table 6

Hadron type	D^+	D^-	D^0	$\bar{D}^0$	Λ_c^+	$\bar{\Lambda}_c$
event %	12.8	23.2	27.5	74.5	56.7	0.3

It is seen, that even without taking into account the mechanism of intrinsic charm release, at low energies channel (2) prevails, while the contribution of channels (3) and (4) is rather small. $\bar{D}^0$-mesons are produced most frequently among charm mesons.

Taking into account the efficiencies of charm hadron decay mode reconstruction which are given in Table 4 and supposing, that losses because of the equipment failures make 30% and 30% of the registered charm decays can not be reconstructed for technical reasons. The following numbers of the completely reconstructed hadron decays of D-mesons and Λ_c^+-baryons may be expected as a result of a 30-day exposure of the SVD in a proton beam with the intencivity of 3×10^6 p/s:

Table 7

Decay modes of D-мesons	Decay probabil. %	Number of reconstructed decays D-мes.	$\bar{D}$-мes.	Decay modes of Λ_c^+-baryon	Decay probabil. %	Number of reconstruct. decays
$D^+ \to \bar{K}^0\pi^+$	2.8	40	70	$\Lambda_c^+ \to p\bar{K}^0$	2.1	210
$\to K^-\pi^+\pi^+$	9.1	580	1050	$\to pK^-\pi^+$	4,4	1500
$\to \bar{K}^0\pi^+\pi^0$	9.7	60	110	$\to p\bar{K}^0\pi^+\pi^-$	2.4	230
$\to \bar{K}^0\pi^+\pi^+\pi^-$	7.0	110	200	$\to \Sigma^+\pi^-\pi^+$	3.0	300
$\to K^-\pi^+\pi^+\pi^0$	6.4	130	240	$\to \Lambda\pi^+\pi^+\pi^-$	2.7	410
$\to \bar{K}^-\pi^+\pi^+\pi^+\pi^-$	0.8	50	90	$\to \Lambda\rho^+$	$2^{(*)}$	200
$D^0 \to K^-\pi^+$	4.0	520	1400			
$\to \bar{K}^0\pi^+\pi^-$	5.3	220	590			
$\to K^-\pi^+\pi^0$	13.8	680	1850			
$\to K^-\pi^+\pi^+\pi^-$	8	1120	3040			
$\to K^-\pi^+\pi^+\pi^-\pi^0$	4.3	180	490			

(*) – theoretical estimation.

In the case, if the cross section of charm production in pN–interactions at 70 GeV/c is significantly smaller, than the expected one, in order to accumulate the statistics sufficient to decide the physical tasks, given in this Proposal, an increase of a beam intensity will be required. As results from the upgraded SVD description, made in the previous Sections, the main detectors of the apparatus can efficiently detect a number of interactions per second, exceeding the one given in Table 4, by a factor of 3–4.

6. THE EXPERIMENTAL PROGRAM AND BEAM–TIME REQUEST

The proposed upgrade of the set-up for the 2nd stage of the experiment E–161 may have been fulfilled for 2–2.5 years from the start of funding with a gradual putting into operation of separate systems of the set-up.

For the first year the main equipment and materials, including computer engineering and electronics components, must have been bought.

For the second year the information collection system must have been put into operation, as well as the upgraded magnetic spectrometer, the detector of γ-quanta, the trigger scintillation hodoscope and the Čerenkov counter.

For the third year the precision vertex detector, block of minidrift tubes and system of trigger electronics will have been accomplished and tested.

In order to carry out the methodical investigations and to test the set-up systems, three test runs per year, each lasting 20–30 shifts, are required during these three years.

To accumulate the main statistics of the experiment (about 30000 completely reconstructed charm decays) three runs at the proton synchrotron U-70, each lasting 100 shifts, are required.

For the primary processing of the statistics, obtained during these runs, about 5000 hours of processor time of an ALFA–type computer is required and the same time for complete reconstruction of the events is needed.

The processing will be carried out in JINR, NPI MSU and IHEP in the equal shares.

References

[1] Andryischin A.M. et al., IHEP Preprint 84-3(1984).

[2] The SVD-Collaboration "Charm production at 70 GeV/c in proton-proton interactions", Proceeding of XXVII Int. Conf. on High Energy Physics, Glasgow, UK, (20-27 July 1994),p.1029.

[3] Appel J.A., Ann.Rev.Nucl.Part.Sci., 42(1992)367.

[4] Tavernier S.P.K., Report on Progress in Physics, 50(1987)1439.

[5] Blumlein J. et al., Phys.Lett., B279(1992)405.

[6] Adamovich et al., Phys.Lett. B284(1992)453.

[7] Alves G.A. et al., Phys.Rev.Lett., 70(1993)722.

[8] Alves G.A. et al., Phys.Rev., D49(1994)R4317.

[9] Badier J. et al., Z.Phys., C20(1983)101.

[10] Alde D.M. et al., Phys.Rev.Lett., v.66(1991)133.

[11] Ashman J. et al., Phys.Lett., B202(1988)603.

[12] Blaizot P. and Ollitrault J.Y., Phys.Lett., B217(1989)386.

[13] Biino C. et al., Phys.Rev.Lett., 58(1987)2523.

[14] G.Bodwin, Phys.Rev., D31(1985)2616.

[15] M.Aguilar–Benitez et al., Z.Phys., C31(1986)491.

[16] Adamovich et al., Phys.Lett. B305(1993)402.

[17] Alves G.A. et al., Phys.Rev.Lett.,v.72(1994)812.

[18] Vogt R., Brodsky S.J., Preprint SLAC-Pub-6468, LBL-35380, 1994.

[19] S.J.Brodsky et al., Phys.Lett., 93B(1980)451.

[20] Vogt R. et al., Nucl.Phys., B383(1992)643.

[21] J.J.Aubert et al., Nucl.Phys., B213(1983)31.

[22] Hoffman E. and Moore R., Z.Phys., C20(1983)71. Golubkov Yu.A., Preprint DESY 94-060(1994).

[23] Chao W.Q. et al., Preprint CCAST-95-09(1995).

[24] Ingelman G., Schlein P., Phys.Lett.152B(1985)256.

[25] Zmushko V.V., IHEP Preprint 95-79(1995).

[26] Mangano M.L. et al., Nucl.Phys.,B405(1993)507.

[27] Barlag S. et al., Phys.Lett.,B302(1992)112.

[28] Aoki S. et al., Prog.Theor.Phys.,v.87(1992)1315.

[29] Adamovich M. et al., Preprint CERN/PPE94-214(1994).

[30] Bogolyubsky M.Yu. et al., YA.F.,v.44(1987)1032.

[31] Kamal A.N., Phys.Rev.,(1986)D33,1344.

[32] Kamal A.N. and Verma R.C., Phys.Rev.,D35(1987)3115.

[33] Lipton R., FNAL preprint FERMILAB-Conf-92/06 (1992).

[34] Körner J.G. and Siebert H.W., Annu.Rev.Part.Sci,41(1991)511.

[35] Lee B.W. et al., Phys.Rev.,D15(1977)157.

[36] Körner J.G. et al., Z.Phys.,C2(1991)117.

[37] Körner J.G. and Kramer M., Preprint DESY 92-049(1992).

[38] Xu Q.P. and Kamal A.N., Phys.Rev.,D46(1992)270.

[39] Cheng H.X., Tseng B., Phys.Rev.,D46(1992)1042.

[40] Zenczykowski P., Preprint of INP Krakow 1643/PH (1993).

[41] Verzocchi M., NIM,A351(1994)222.

[42] Frabetti P.L. et al., Phys.Lett., 251B(1990)639.

[43] Bychkov V.N. et al., JINR Preprint E-13-94-351(1994).

[44] Bogdanova G.A. et al., "Multiwire proportional chambers of the SVD apparatus", NPI MSU Preprint (to be published).

[45] Basiladze S.G. et al., The Collection "Hard- and soft-ware of the system of autmatization for the experimental investigations", Publishing house of MSU, 1986,p.120.

[46] Lassale J.-C. et al., NIM,176(1980)371.

[47] Alde D. et al., NIM,240(1985)343.

[48] Baland J.F. et al., Nucl.Phys. B(Proc.Suppl.) 1B(1988)303.

[49] Darbo G., Rossi L., Nucl.Instr.Meth.,A289(1990)584.

[50] Bogolyubsky M.Yu. et al., IHEP Preprint 91-172(1991).

[51] Bogolyubsky M.Yu. et al., Communication of JINR, P1-95-166, Dubna, 1995.

[52] Bogolyubsky M.Yu. et al., JINR preprint, P1-95-451, Dubna, 1995.

Received November 14, 1996

Е.Н.Ардашев, М.Ю.Боголюбский, Н.К.Булгаков и др.
Предложение эксперимента по изучению механизмов образования очарованных частиц в pA-взаимодействиях при 70 ГэВ/с и их распадов.

Оригинал-макет подготовлен с помощью системы LaTeX.
Редактор Е.Н.Горина. Технический редактор Н.В.Орлова.

Подписано к печати 26.11.96. Формат 60 × 84/8. Офсетная печать.
Печ.л. 5,87. Уч.-изд.л. 4,51. Тираж 240. Заказ 900. Индекс 3649.
ЛР №020498 06.04.92.

ГНЦ РФ Институт физики высоких энергий
142284, Протвино Московской обл.